Materials Today Bio 12 (2021) 100155

Contents lists available at ScienceDirect

Materials Today Bio

journal homepage: www.journals.elsevier.com/materials-today-bio

Fatty acid synthase as a feasible biomarker for triple negative breast cancer stem cell subpopulation cultured on electrospun scaffolds

Marc Rabionet [a,b], Emma Polonio-Alcalá [a,b], Joana Relat [c,d,e], Marc Yeste [f], Jennifer Sims-Mourtada [g], April M. Kloxin [h], Marta Planas [i], Lidia Feliu [i], Joaquim Ciurana [b,**], Teresa Puig [a,*]

[a] New Therapeutic Targets Laboratory (TargetsLab) - Oncology Unit, Department of Medical Sciences, Faculty of Medicine, University of Girona, Emili Grahit 77, 17003, Girona, Spain
[b] Product, Process and Production Engineering Research Group (GREP), Department of Mechanical Engineering and Industrial Construction, University of Girona, Maria Aurèlia Capmany 61, 17003, Girona, Spain
[c] Department of Nutrition, Food Sciences and Gastronomy, School of Pharmacy and Food Sciences, Food and Nutrition Torribera Campus, University of Barcelona, Prat de la Riba 171, 08921, Santa Coloma de Gramenet, Spain
[d] Institute of Nutrition and Food Safety of the University of Barcelona (INSA-UB), E-08921 Santa Coloma de Gramenet, Spain
[e] CIBER Physiopathology of Obesity and Nutrition (CIBER-OBN), Instituto de Salud Carlos III, E-28029 Madrid, Spain
[f] Biotechnology of Animal and Human Reproduction (TechnoSperm), Department of Biology, Institute of Food and Agricultural Technology, University of Girona, Pic de Peguera 15, 17003, Girona, Spain
[g] Center for Translational Cancer Research, Helen F Graham Cancer Center and Research Institute, Christiana Care Health Services, Inc, Newark, DE, USA
[h] Chemical and Biomolecular Engineering, University of Delaware, Newark, DE, 19716, USA
[i] LIPPSO, Department of Chemistry, University of Girona, Maria Aurèlia Capmany 69, 17003, Girona, Spain

ARTICLE INFO

Keywords:
Triple negative breast cancer
Three-dimensional cell culture
Polycaprolactone
Electrospun scaffolds
Breast cancer stem cells
Fatty acid synthase

ABSTRACT

There is no targeted therapy for triple negative breast cancer (TNBC), which presents an aggressive profile and poor prognosis. Recent studies noticed the feasibility of breast cancer stem cells (BCSCs), a small population responsible for tumor initiation and relapse, to become a novel target for TNBC treatments. However, new cell culture supports need to be standardized since traditional two-dimensional (2D) surfaces do not maintain the stemness state of cells. Hence, three-dimensional (3D) scaffolds represent an alternative to study *in vitro* cell behavior without inducing cell differentiation. In this work, electrospun polycaprolactone scaffolds were used to enrich BCSC subpopulation of MDA-MB-231 and MDA-MB-468 TNBC cells, confirmed by the upregulation of several stemness markers and the existence of an epithelial-to-mesenchymal transition within 3D culture. Moreover, 3D-cultured cells displayed a shift from MAPK to PI3K/AKT/mTOR signaling pathways, accompanied by an enhanced EGFR and HER2 activation, especially at early cell culture times. Lastly, the fatty acid synthase (FASN), a lipogenic enzyme overexpressed in several carcinomas, was found to be hyperactivated in stemness-enriched samples. Its pharmacological inhibition led to stemness diminishment, overcoming the BCSC expansion achieved in 3D culture. Therefore, FASN may represent a novel target for BCSC niche in TNBC samples.

1. Introduction

Breast cancer (BC) is the most common cancer among women worldwide, accounting for 2.1 million diagnoses in 2018 as stated by the International Agency for Research on Cancer [1]. Among the different BC clinical subtypes, the Triple Negative Breast Cancer (TNBC) is characterized by the lack of estrogen and progesterone receptors and no overexpression of human epidermal growth factor receptor-2 (HER2), contrary to the other subtypes which overexpress at least one of these markers [2]. This fact prevents the use of targeted therapies and leaves

* Corresponding author.
** Corresponding author.
E-mail addresses: m.rabionet@udg.edu (M. Rabionet), emma.polonio@udg.edu (E. Polonio-Alcalá), jrelat@ub.edu (J. Relat), marc.yeste@udg.edu (M. Yeste), JSimsMourtada@ChristianaCare.org (J. Sims-Mourtada), akloxin@udel.edu (A.M. Kloxin), marta.planas@udg.edu (M. Planas), lidia.feliu@udg.edu (L. Feliu), quim.ciurana@udg.edu (J. Ciurana), teresa.puig@udg.edu (T. Puig).

https://doi.org/10.1016/j.mtbio.2021.100155
Received 2 July 2021; Received in revised form 2 November 2021; Accepted 5 November 2021
Available online 16 November 2021

systemic chemotherapy as the sole treatment option for TNBC patients [3], even though recent efforts have been made in the field of conjugated drugs and nanoparticles [4,5]. Nevertheless, TNBC accounts for 15–20% of the BC cases [6] and displays a very aggressive profile. TNBC patients are younger, present a higher relapse rate, and exhibit a greater incidence of metastasis and higher mortality among BC subtypes [7]. Unfortunately, despite a very good initial treatment response, there is a 40% of relapse risk in the case tumor is not properly eradicated [8]. Within TNBC cells, two main molecular subtypes are represented, basal-like (80%) and mesenchymal-like (also known as claudin-low; 20%), the latter being enriched in stem-like features [9].

Relapse appearance and therapeutic failure are caused in part by cells within the tumor that display stem-like properties, thus termed breast cancer stem cells (BCSCs). Different studies described this subset as a tumor-initiating subpopulation which exhibits radio- [10] and chemo-resistance, showing self-renewal capacity and favoring tumor recurrence. Since this malignant subpopulation shares some characteristics similar to mammary stem cells, BCSCs also express pluripotency, self-renewal, and stemness markers such as SOX2, SOX4, NANOG, and CD49f [11]. *In vitro*, BCSCs possess the capacity to grow in non-adherent conditions forming suspended mammospheres [12] and an enhanced aldehyde dehydrogenase 1 (ALDH1) enzyme activity [13]. The $CD44^{+}/CD24^{-/low}$ cell-surface marker pattern has also been used to isolate BCSCs [14]. Besides, epithelial-to-mesenchymal transition (EMT) is known to confer stem-like traits on non-stem cells, facilitating the generation of BCSCs [15]. EMT is a well-regulated cell program during embryogenesis and is responsible for the development of many tissues [16]. However, cancer epithelial cells can undergo EMT losing epithelial cell polarity and acquiring mesenchymal abilities, such as invasion and migration [17], which can ultimately lead to metastasis. EMT comprises different molecular alterations including the upregulation of several transcription factors such as SNAIL, SLUG, ZEB1, ZEB2, and TWIST. During the acquisition of mesenchymal properties, cells adopt a more invasive phenotype via downregulation of E-cadherin, as this protein is involved in the establishment of cell-cell adhesion [18]. This fact is accompanied by the overexpression of the mesenchymal protein vimentin, which contributes to cytoskeleton organization and focal adhesion stability [19].

Along with BCSC presence, it is known that cancer cells also suffer from metabolism deregulation to deal with the high demand of the uncontrolled cell growth. In particular, the enzyme fatty acid synthase (FASN) is found overactivated in cancer cells in contrast with its low expression in normal tissue (except in lipogenic tissues such as liver, adipose tissue [20], and lactating mammary glands [21]), where diet regulates its expression. In cancer cells, FASN is responsible for the synthesis of almost all the fatty acids *de novo* [22], mainly phospholipids which can act not only as structural pieces but also as signaling molecules [23]. For this reason, FASN has become a unique oncologic target whose inhibition has been demonstrated to hinder tumor progression [24–26] and overcome resistance to chemotherapeutic agents [27,28], by disrupting lipid membrane synthesis, protein palmitoylation, and signaling of major oncogenic pathways [29]. (−)-Epigallocatechin-3-gallate (EGCG), the most abundant catechin in green tea, belongs to the early generation of FASN inhibitors [30]. Despite its effect on EGFR-HER2, MAPK, and PI3K/AKT/mTOR signaling pathways among others, apoptosis after EGCG treatment occurs through FASN inhibition [25,31]. The aforementioned off-target toxicity, along with other bioavailability limitations, led to the production of new FASN inhibitors. For instance, the EGCG-analogue G28 shows more specificity and enhanced FASN inhibitory activity [32], even in TNBC models [33]. In fact, mounting evidence supports that lipid metabolism disorders exert a great impact on CSC niche. Overexpression of FASN was detected on induced pluripotent stem cells [34] and its expression has been associated with the level of stemness markers in glioma stem cells [35]. Its inhibition has led to the decrease of several stemness features [35–38], indicating a role in stemness maintenance. Taking all this into account, FASN is suggested to be a more vulnerable target in CSCs than in normal cancer cells [39].

Despite the importance of BCSCs in the oncologic research field, their investigation faces some limitations. They represent a low percentage within the tumor or cell line [14,40] and, most importantly, *in vitro* two-dimensional (2D) cell culture surfaces induce their differentiation, losing their stem-like state [41]. In 2D supports, cells can only grow by forming a monolayer, adopting a flattened morphology which results in cytoskeleton remodeling. Cell shape variations can modify gene and protein expression [42,43] leading to, for instance, BCSC differentiation. Aside from the lack of three-dimensionality, stiffness also represents a significant gap between traditional *in vitro* cell culture supports and physiological surroundings. Mammalian cells are generally attached to soft surfaces such as another similar cell or the extracellular matrix (ECM), in contrast with the rigidity of 2D surfaces used for *in vitro* studies [44]. It has been reported that microenvironment stiffness can have a great mechanical impact on the cell, including changes in morphology, motility, proliferation, protein expression, and spreading [45,46]. Besides, ECM stiffness plays a crucial role in regulating stem cell self-renewal and differentiation. For instance, a soft matrix was proved to increase the stem-like niche of breast cancer cells, including TNBC cell lines [47,48]. Three-dimensional (3D) cell culture supports have emerged as an alternative to reinstate a physiological-like structure and overcome the above-mentioned issues. Among them, fibrous scaffolds offer a physical structure made by a network of polymeric filaments, which mimics ECM architecture, plenty of fibrous proteins such as collagen and elastin [49]. Over the past decade, electrospinning (ES) technology has been proposed to fit scaffold manufacturing demands thanks to its customizability and the capacity to fabricate small diameter fibers [50,51]. This manufacturing process, combined with the use of viscoelastic and biocompatible polymers such as poly(ε-caprolactone) (PCL) [52], allows the production of ECM-like structures suitable for 3D cell culture. Interestingly, a previous investigation revealed that the use of 15% PCL ES scaffolds enhanced the mammosphere forming capacity and ALDH activity of the TNBC MDA-MB-231 cell line, indicating a BCSC expansion [53]. This fact, corroborated by more works which used scaffolds for expanding cancer stem features [54–56], empowers the use of PCL scaffolds as a 3D culture support to enrich and study BCSC subpopulation.

All things considered, the BCSC population could become a potential target for BC treatment, in particular for TNBC subtype. To overcome *in vitro* limitations, the present study validated the stemness-enriching capacity of 15% PCL ES scaffolds with mesenchymal-like MDA-MB-231 and basal-like MDA-MB-468 TNBC cells. Furthermore, alterations in common signaling pathways were analyzed, and FASN expression and inhibition were evaluated in order to be proposed as a novel biomarker for TNBC stemness-enriched samples. Obtained results demonstrated a FASN hyperactivation in BCSC-enriched 3D TNBC samples, and its inhibition overcame the stemness expansion achieved in 3D culture, suggesting the possibility to inhibit FASN to treat the TNBC stem-like cells.

2. Materials and methods

2.1. Scaffold manufacture

Scaffolds were manufactured through electrospinning technology, as previously described [57]. Briefly, poly(ε-caprolactone) (PCL; 80,000 g/mol; Sigma-Aldrich, St. Louis, MO, USA) and acetone (PanReac AppliChem, Gatersleben, Germany) were used to create a 15% w/v PCL solution. A solution volume of 5 mL was processed through an electrospinning apparatus (Spraybase, Dublin, Ireland) and an 18 G needle emitter located 10 cm above the stationary collector. A voltage of 7 kV was applied and the flow rate was fixed at 6 mL/h by the Syringe Pump Pro software (New Era Pump Systems, Farmingdale, NY, USA). Produced meshes were cut into squares with a scalpel. A previous characterization revealed that scaffolds exhibited a random pattern of fibers with an average diameter of 701.13 ± 401.89 nm, a surface porosity of 22.48 ± 7.57%, and a pore area of 0.84 ± 1.82 μm^2 [53].

2.2. Dynamic mechanical analysis

Scaffold mechanical profile was measured by dynamic mechanical analysis (DMA) employing the Mettler Toledo DMA/SDTA861e instrument (Columbus, OH, USA). Both unsterilized unincubated (UU) and sterilized PCL scaffolds incubated in medium (SI) were processed. PCL meshes were sterilized by immersion into 70% ethanol/water solution overnight, washed three times with phosphate-buffered saline (PBS; Gibco, Waltham, MA, USA) and finally exposed to germicidal UV light for 30 min. Then, they were incubated with Dulbecco's Modified Eagle's Medium (DMEM; Gibco) for 12 days, simulating the maximum culture time performed in the following *in vitro* experiments. DMEM was supplemented with sterile filtered and heat inactivated 10% fetal bovine serum (FBS; collected and processed in USA; HyClone Laboratories, GE Healthcare, Chicago, IL, USA), 1% L-glutamine, 1% sodium pyruvate (Gibco), and 50 U/mL Pen/Strep (Linus, Cultek, Madrid, Spain). Scaffolds were cut into 5.5 mm × 5.5 mm squares with a thickness of 0.33–0.36 mm and a large tension clamp was used as a sample holder. The storage modulus (E′) and tan delta (Tan δ) were analyzed and plotted.

2.3. Three-dimensional cell culture

Mesenchymal-like MDA-MB-231 and basal-like MDA-MB-468 TNBC cells were used in this study. Sterilized scaffolds were placed onto non-adherent cell culture microplates (Sarstedt, Nümbrecht, Germany) and soaked in culture medium for 30 min at 37 °C prior cell seeding to favor cell attachment. Corresponding cell density was prepared in a small volume of medium (see Table S1). Cell suspension was pipetted drop by drop onto the scaffold center. Afterwards, scaffolds were incubated for 3 h at 37 °C and 5% CO_2 atmosphere to allow cell attachment; supplemented DMEM culture medium was subsequently added. For cell detachment, scaffolds were once washed with PBS and transferred into new wells to collect only those cells that attached to PCL filaments. Cells from 2D culture and scaffolds were detached with trypsin-EDTA (Cultek) at 37 °C and 5% CO_2 atmosphere. More details can be found in **SI Appendix**.

2.4. Mammosphere forming assay

After cell detachment, 2,000 cells were seeded onto a 6-well non-adherent cell culture microplate (Sarstedt) and incubated for 7 days at 37 °C and 5% CO_2. Cells were cultured with DMEM/F12 medium (HyClone) supplemented with B27 (Gibco), hEGF and hFGF (20 ng/mL; Milteny Biotec, Bergisch Gladbach, Germany), 1% L-glutamine and 1% sodium pyruvate (Gibco). After incubation, spherical mammospheres with a minimum diameter of 50 μm were counted. The following equation was used to calculate the Mammosphere Forming Index (MFI) of each culture condition:

$$MFI\ (\%) = \frac{n^{\circ}\ mammospheres}{n^{\circ}\ seeded\ cells}\ X\ 100$$

2.5. ALDEFLUOR™ assay

ALDEFLUOR™ kit (STEMCELL Technologies, Vancouver, Canada) was used to determine the ALDH enzyme activity, following the company guidelines. Cells were detached from the culture plastic (2D samples) and PCL scaffolds (3D) as previously described, PBS-rinsed and 200,000 cells were resuspended in 500 μL of ALDEFLUOR™ assay buffer. Afterwards, 2.5 μL of ALDEFLUOR™ Reagent (BAAA) was added to each cell suspension and 250 μL of the suspension was immediately transferred to a new tube with 2.5 μL of the ALDH inhibitor diethylaminobenzaldehyde (DEAB) to consider background fluorescence. All samples were incubated for 45 min at 37 °C in the dark. Cells were then centrifuged, washed, and analyzed with a Cell Lab Quanta flow cytometer (Bechkman Coulter Inc., Miami, FL, USA) to quantify the ALDH-positive cell population. More details can be found in **SI Appendix**.

2.6. Quantitative real-time PCR analysis

Once trypsinized, 2D- and 3D-cultured cells were suspended with 750 μL of Qiazol (Qiagen, Hilden, Germany). Total RNA from each sample was isolated using a RNeasy Mini Kit (Qiagen) following the instructions provided by the manufacturer. After extraction, RNA amount and purity were determined by spectroscopy (NanoDrop™ One Microvolume UV–Vis spectrophotometer, Thermo Fisher Scientific, Waltham, MA, USA). RNA was reverse-transcribed into complementary DNA using High Capacity cDNA Archive Kit (Applied Biosystems, Foster City, CA, USA). Gene expression levels were assessed using QuantStudio 3 Real-Time PCR System (Applied Biosystems) with qPCRBIO SyGreen Mix Lo-ROX (PCR Biosystems, London, UK). Gene expression levels were quantified by double delta Ct analysis method and normalized to the housekeeping gene *GAPDH*. More details can be found in **SI Appendix** and Table S2.

2.7. $CD44^{+}/CD24^{-/low}$ analysis

After detachment, cells were washed with PBS containing 10% FBS and resuspended at a density of 2×10^6 cells/mL in cold PBS with 10% FBS. Cells were stained with allophycocyanin (APC)-conjugated CD44 and fluorescein isothiocyanate (FITC)-conjugated CD24 (Abcam, Cambridge, MA, USA) for 30 min in the dark at room temperature. Samples were centrifuged, washed, and passed through a BD Falcon cell strainer cap tube (BD, Franklin Lakes, NJ, USA) for fluorescence-activated cell sorting analysis. Samples were analyzed on a fluorescence-activated cell sorting LSRFortessa flow cytometer (BD) and were gated on an unstained control. Compensation was performed with single stained cells to decrease overlaps of fluorophore emission spectrums.

2.8. Western blot

After culture, the cell pellet was PBS-rinsed and lysed in ice-cold lysis buffer (Cell Signaling Technology, Inc., Danvers, MA, USA) with 100 μg/mL phenylmethylsulfonyl fluoride (PMSF; Sigma-Aldrich) by vortexing every 5 min for 30 min. Total protein content of each lysate was determined by Lowry-based DC Protein Assay (Bio-Rad Laboratories, Inc., Hercules, CA, USA). Equal amounts of protein (10 μg) were heated in Lithium Dodecyl Sulfate (LDS) Sample Buffer with Sample Reducing Agent (Invitrogen, Carlsbad, CA, USA) for 10 min at 70 °C, electrophoresed on 7.5% sodium dodecyl sulfate polyacrylamide gels (Bio-Rad Laboratories, Inc.), and transferred onto nitrocellulose membranes (Thermo Fisher Scientific). Blots were incubated at room temperature for 3 h in blocking buffer [5% bovine serum albumin (BSA) in tris-buffered saline with 0.1% Tween (TBS-T)] to avoid non-specific antibody binding. Afterwards, membranes were incubated overnight at 4 °C with the appropriate primary antibody diluted in blocking buffer (see Table S3). Specific horseradish peroxidase (HRP)-conjugated secondary antibody was incubated for 1 h at room temperature. Immune complexes were detected using a chemiluminescent HRP Substrate [Clarity™ Western ECL Substrate (Bio-Rad Laboratories, Inc.) or SuperSignal™ West Femto (Thermo Fisher Scientific)] and a ChemiDoc™ Imaging System (Bio-Rad Laboratories, Inc.). Western blot analyses were repeated at least three times and representative results are shown. Protein bands were quantified by densitometric analysis using Image Lab™ Software (Bio-Rad Laboratories, Inc.). The expression ratios were determined after normalizing against individual GAPDH levels.

2.9. FASN activity

Cells were cultured on 2D wells and 3D scaffolds for 6 days as previously described in 2.3 section. For the last 6 h, medium was replaced by

DMEM supplemented with 1% lipoprotein-deficient FBS (Sigma-Aldrich) and 0.5 μCi/mL (1,2–^{14}C) acetic acid sodium salt (53.9 mCi/mmol; Perkin Elmer Biosciences, Waltham, MA, USA). Cells were harvested and washed twice with PBS (500 μL) and once with methanol:PBS (2:3; 500 μL). The pellet was resuspended in 0.2 M NaCl (100 μL) and lysed with freeze-thaw cycles. Lipids from cell debris were extracted by centrifugation (2000 G, 5 min) with chloroform:methanol (2:1; 350 μL) and KOH 0.1 M (25 μL). The organic phase recovered was then washed with chloroform:methanol:water (3:48:47; 100 μL) and evaporated in a Speed-vac Plus SC110A (Savant Instruments Pvt. Ltd., Hyderabad, India). The dried pellets were resuspended in ethanol and transferred to a vial for radioactive counting. Total protein content in cell debris was quantified with the Bradford assay (Thermo Fisher Scientific).

2.10. Cell viability assay

After 6 days of culture on 2D and 3D supports, complete medium (including serum) along with the corresponding concentrations of doxorubicin (TEDEC-Meiji Farma, Alcalá de Henares, Spain), paclitaxel (Accord Healthcare Ltd., Thaltej, India), EGCG (Sigma-Aldrich) or G28 were added to the cultures. Following a 48-h treatment, a colorimetric MTT assay (3-(4,5-dimethyl-2-thiazolyl)-2,5-diphenyl-2H-tetrazolium bromide; Sigma-Aldrich) was used to measure cell viability. More details can be found in **SI Appendix**.

2.11. Statistical analysis

All data are expressed as mean ± standard error of the mean (SEM). Data were analyzed using IBM SPSS (SPSS Inc., Chicago, IL, USA). When data normality and homogeneity of variances were confirmed through Shapiro-Wilk and Levene tests, a linear mixed model followed by post-hoc Sidak test were carried out. If data did not fulfil with parametric assumptions, they were tested with Scheirer-Ray-Hare and Mann-Whitney tests. The level of significance was set at $p < 0.05$. All observations were confirmed by at least three independent experiments.

3. Results and discussion

3.1. Stiffness characterization of electrospun PCL scaffolds

Most stiffness studies have been performed using hydrogels, and viscoelastic features when using nanofiber PCL scaffolds have been usually neglected. Since stiffness of the cell culture support can have a great impact on the cell, a dynamic mechanic analysis (DMA) was performed on 15% PCL scaffolds to characterize their viscoelastic behavior. Unsterilized unincubated (UU) scaffolds were analyzed, as well as sterilized scaffolds incubated with culture medium (SI) in order to consider the possible effect of EtOH/UV sterilization and incubation processes on the specimens' stiffness. Scaffolds were kept in medium for 12 days, simulating the maximum culture time performed in the following *in vitro* experiments.

Elastic response of the material can be defined by the storage modulus (E′), shown in Fig. 1A and B, which measures the capacity of the material to store elastic energy. UU meshes showed an E′ value of approximately 9.18 MPa at room temperature (25 °C) and around 7.33 at a physiological one (37 °C). Besides, measures from SI scaffolds did not show significant differences, with values of 11.76 MPa (at 25 °C) and 9.68 MPa (at 37 °C). Meanwhile, E′ values from polystyrene (PS), the main component of 2D culture surfaces, are reported to range from 1,300 to 3,000 MPa at room temperature in the literature [58,59]. Hence, lower E′ values of PCL meshes indicate that this material shows reduced solid-like properties and lower strength and mechanical rigidity. Consequently, produced PCL

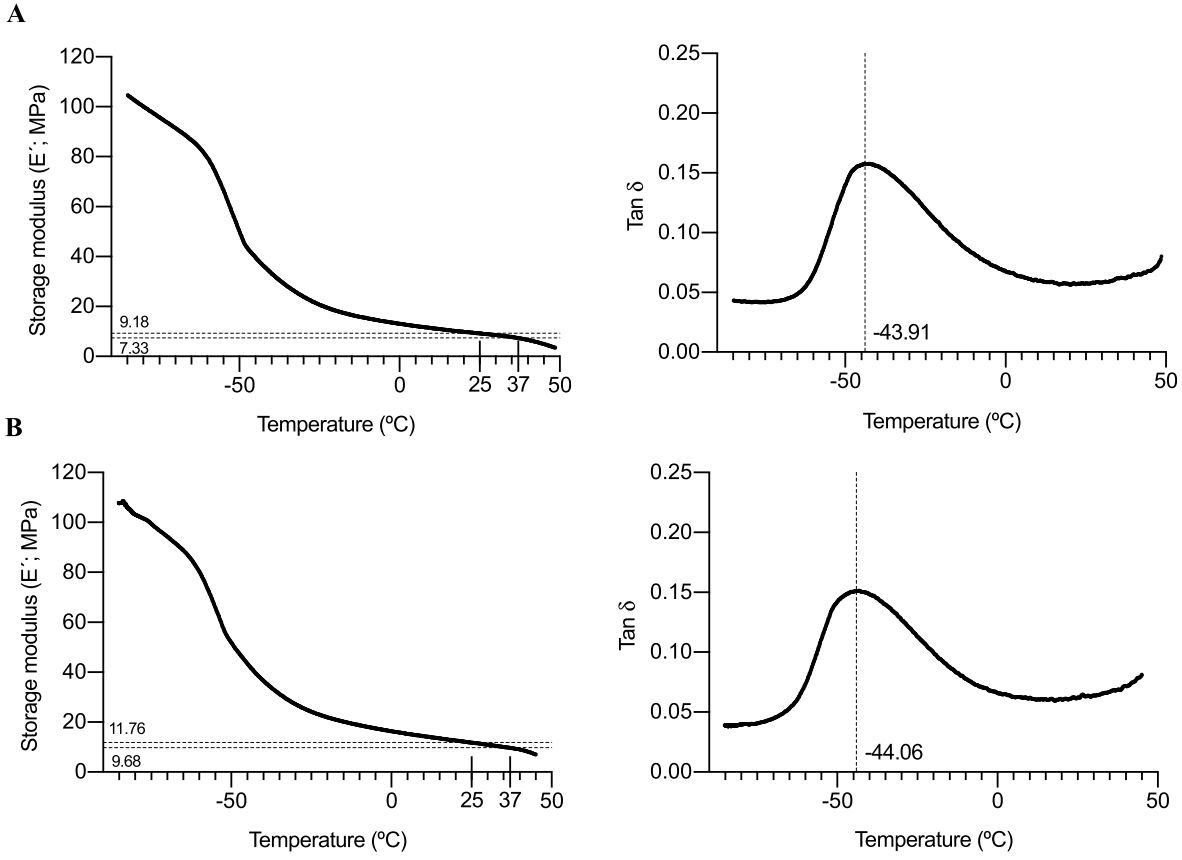

Fig. 1. Dynamic Mechanical Analysis (DMA) for 15% PCL scaffolds. Storage modulus and Tan δ of unsterilized unincubated scaffolds (**A**) and sterilized scaffolds incubated with culture medium for 12 days (**B**) were plotted against temperature.

scaffolds represent a softer cell culture support, although they are stiffer compared with breast cancer tissue, whose E' values vary from 10 to 40 kPa [60]. Previous studies using fibroblasts reported that cells generate more traction force and develop a broader and flatter morphology on stiff surfaces [45]. In this context, cell responses on PCL nanofibers are likely influenced by both the stiffness and three-dimensionality of these fibers, where elongated morphologies have been observed for MDA-MB-231 and MDA-MB-468 cells in previous studies [53,61].

The loss tangent (or tan delta; Tan δ) is the ratio of loss modulus (E″) and storage modulus (E′), which indicate the viscosity of material and elastic properties, respectively. Interestingly, Tan δ curve peak designates the polymer's glass transition temperature (T_g), the critical temperature at which the transition between glassy and rubbery state occurs [62]. As seen in Fig. 1A and B, UU PCL scaffolds exhibited a glass transition point of −43.91 °C while SI meshes showed a non-statistically different value of −44.06 °C, similar to the one of neat PCL (−60 °C) [63], and other PCL structures used in the literature [64,65]. Consequently, when working at room or physiologically temperature, 3D PCL scaffolds are above their T_g, exhibiting a more elastic profile compared with PS, whose T_g value is around 100 °C [66].

Interestingly, UU and SI scaffolds showed a similar behavior through DMA analyses, indicating that neither the EtOH/UV sterilization process nor the medium incubation at 12 days maximum modify E' or tan delta values and, therefore, their viscoelastic profile.

3.2. Impact of scaffold culture on MDA-MB-468 BCSC subpopulation

Scaffold-induced enrichment of BCSC population was previously reported by our research group using mesenchymal-like TNBC MDA-MB-231 cell model, which exhibited an elongated cytoplasm, greater mammosphere forming capacity, and a 3.4-fold increased ALDH activity after 3D culture [53]. Furthermore, basal-like TNBC MDA-MB-468 cells were proved to adopt a more elongated morphology in ES PCL scaffolds, in disagreement with the flattened morphology on 2D cultures [61]. For this reason, we used the same random PCL 700 nm diameter nanofibers model to culture MDA-MB-468 cell line and analyze the impact on BCSCs through mammosphere forming assay, ALDH activity, and $CD44^{+}/CD24^{-/low}$ proportion. As shown in Fig. 2A, cells after 3D culture displayed a significantly higher mammosphere forming index (MFI) when compared with the pertinent monolayer culture, regardless of cell culture time. Moreover, no significant differences were observed within the same cell culture support over time. A time-dependent trend was observed on the ALDH activity (Fig. 2B). At early time points (3 and 6 culture days) cells from scaffolds possessed a larger ALDH+ subpopulation compared to 2D control. However, after 12 days of incubation the trend was the opposite due to a hyperactivation of ALDH activity on monolayer cells. Representative dot plots are given in Table S4. While mRNA *CD44* levels remained broadly stable, lower *CD24* expression was observed in scaffolds culture compared with monolayer control (Fig. 2C), which is correlated with increased tumorigenicity [14,67]. To confirm

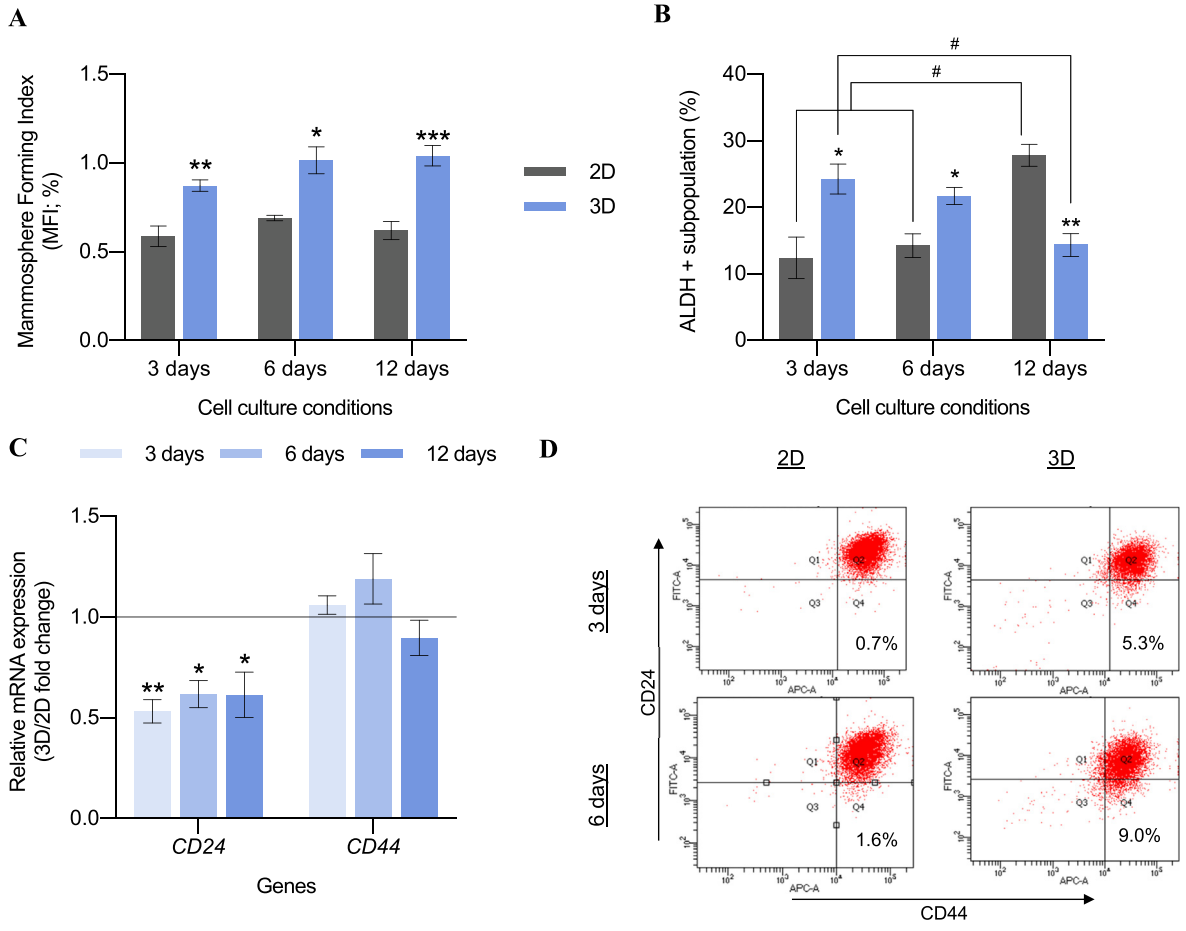

Fig. 2. MDA-MB-468 stemness features after monolayer (2D) and 15% PCL scaffolds (3D) culture. A mammosphere forming assay (**A**), ALDEFLUOR assay (**B**), CD24 and CD44 mRNA expression profile (**C**), and protein expression pattern of CD24/CD44 (**D**) are depicted. Gene expression levels were quantified by double delta Ct analysis method and normalized to the housekeeping gene *GAPDH*. Cells were incubated with CD44-APC and CD24-FITC antibodies. Percentage of breast cancer stem-like cells ($CD44^{+}/CD24^{low/-}$) is represented in Q4. Data are representative of three separate experiments. Significant differences of 3D with regard to corresponding 2D cultures are indicated as * ($p < 0.05$), ** ($p < 0.01$) and *** ($p < 0.001$). Significant differences of culture time within same culture support are indicated as # ($p < 0.05$).

these data, the expression of CD24 and CD44 cell surface markers was assessed through flow cytometry (Fig. 2D). An increase in the $CD44^{+}/CD24^{-/low}$ population was observed after 3 and 6 days of culture compared with 2D samples. Taking all this into consideration, 3D scaffold culture enlarged the percentage of BCSC-like $CD44^{+}/CD24^{-/low}$ cells, with decreasing CD24 expression levels, since its basal population was mainly $CD44^{+}/CD24^{+}$. Overall, 3D culture on ES 15% PCL scaffolds caused an enrichment of the BCSC subpopulation in the basal-like MDA-MB-468 cell model, especially at early culture times, following the effect previously reported with the mesenchymal-like MDA-MB-231 cells [53].

3.3. Stemness markers expression and chemoresistance of TNBC models cultured on scaffolds

More stemness features were further analyzed to confirm the expansion of the breast cancer stem cell population when scaffolds were used with the MDA-MB-231 and MDA-MB-468 TNBC models. Expression of the stemness-related genes *SOX2*, *SOX4*, *NANOG* and *CD49f* were examined along time in 2D and 3D-cultured cells (Fig. 3). SOX2 is a transcription factor involved in pluripotency maintenance and self-renewal capacity [68]. In tumoral tissues, it plays a key role in differentiation, invasion, metastasis, and drug resistance [69]. SOX4 is another transcription factor related to development processes and progression of

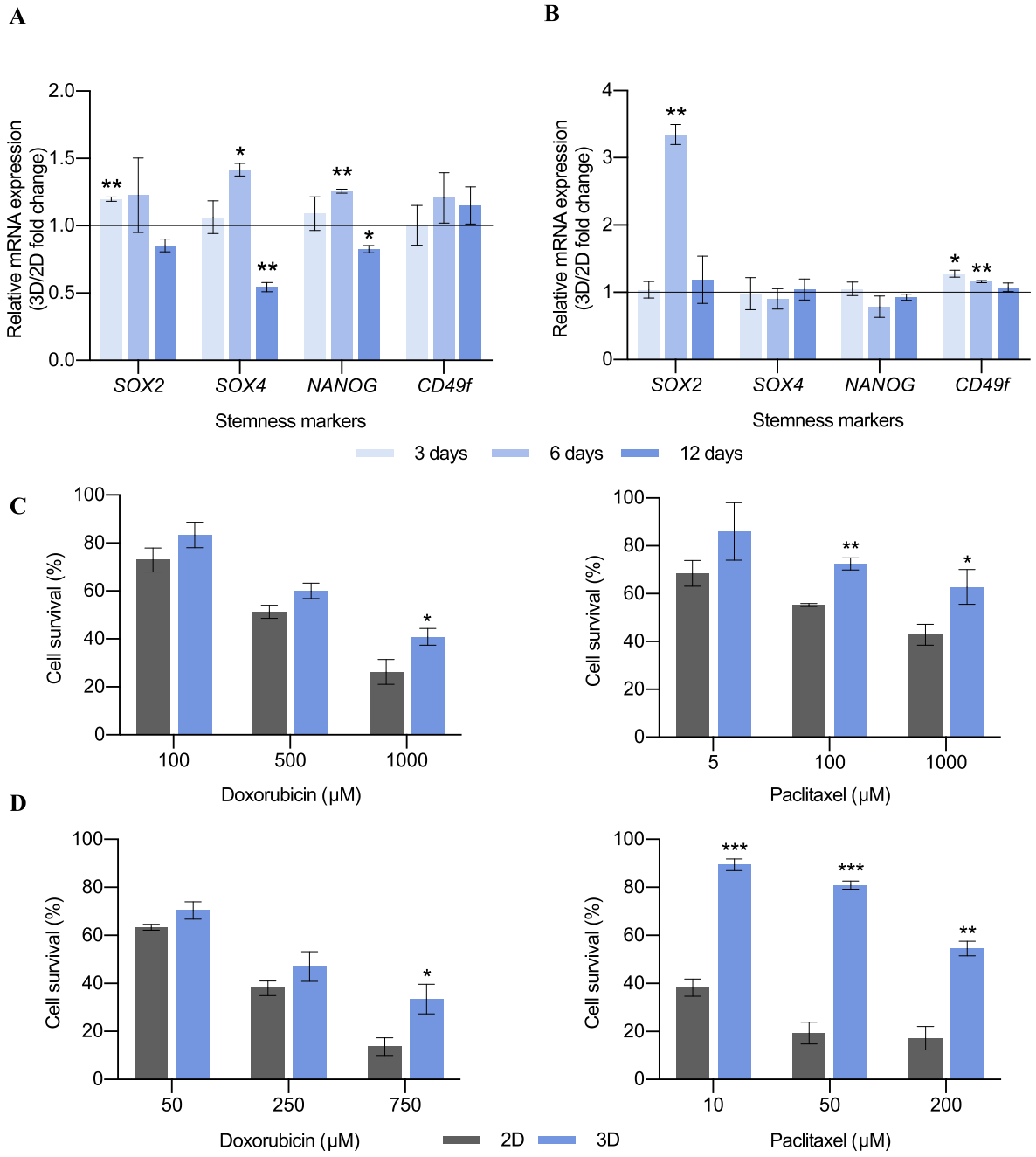

Fig. 3. Stemness features expression analysis. Fold changes in mRNA levels of stemness-related genes in 3D-cultured cells compared to corresponding 2D control for MDA-MB-231 (**A**) and MDA-MB-468 (**B**) cell models. Gene expression levels were quantified by double delta Ct analysis method and normalized to the housekeeping gene *GAPDH*. Cell survival plots for MDA-MB-231 (**C**) and MDA-MB-468 (**D**) cell models are also depicted. Cells were cultured on monolayer (2D) or in PCL scaffolds (3D) for 6 days and then exposed to the chemoagents doxorubicin or paclitaxel for 48 h. Data are expressed as percentage of untreated cells as determined by MTT assay. Significant differences of 3D with regard to 2D cultures are indicated as * ($p < 0.05$), ** ($p < 0.01$) and *** ($p < 0.001$).

cancer [70], and it is used as a CSC-specific marker [55]. NANOG is a key transcription factor involved in self-renewal and pluripotency maintenance in embryonic stem cells. Moreover, it is thought to be regulated by the cooperative action of SOX2 and OCT3/4 [71]. CD49f was found to possess a key role in stemness maintenance through direct regulation of OCT3/4 and SOX2 [72]. MDA-MB-231 cells cultured on scaffolds showed an upregulation of *SOX2* after 3 days of culture, and an overexpression of *SOX4* and *NANOG* after 6 days (Fig. 3A). On the other hand, scaffold culture led to an upregulation of *SOX2* and *CD49f* levels on MDA-MB-468 cell model (Fig. 3B). Interestingly, *SOX2* and *SOX4* have been related to mammosphere forming capacity [73,74]. However, long incubation periods on scaffolds did not result in the activation of any stemness-related gene and even a downregulation was observed in the case of the mesenchymal-like model (Fig. 3A). Therefore, the upregulation of several stemness-related markers proved the BCSC enrichment found in 3D culture at early times.

Another intrinsic characteristic of the BCSC niche is the increased resistance to chemotherapy [75]. Concretely, it has been shown that BCSCs display resistance to doxorubicin and paclitaxel [76,77], two therapeutic agents currently used against TNBC [78]. Since the majority of stemness features were found to be upregulated after 6 days of culture in 3D scaffolds, chemoresistance was evaluated at this time. MDA-MB-231 and MDA-MB-468 cells were cultured in tissue culture plastic and 3D 15% PCL scaffolds for 6 days and they were later treated with doxorubicin and paclitaxel for 48 h. As seen in Fig. 3C and D, both cell models exhibited a significant higher cell survival rate when cultured in scaffolds compared with monolayer culture, after treatment with the two chemoagents. Greater differences between 2D and 3D samples were observed when higher drug concentrations were used, in agreement with other studies [56]. SOX2, whose expression was upregulated in both cell models when cultured in scaffolds (Fig. 3A and B), was linked to drug resistance [69]. More specifically, it was found to play a key role in paclitaxel resistance [79], explaining the greatest cell survival of 3D-cultured MDA-MB-468 cells after paclitaxel addition; since this model was the one exhibiting the highest *SOX2* expression (Fig. 3B). Chemoresistance can be partially explained by the overexpression of multidrug resistance (MDR) pumps [80], previously related to BCSC expression [81]. Concretely, MDA-MB-231 3D-cultured cells expressed significantly higher levels of *ABCG2*, whereas MDA-MB-468 model exhibited an enlarged gene expression of the *ABCB1* pump (whose exogenous substrate is paclitaxel [82]) when seeded on scaffolds (Fig. S1).

3.4. Epithelial-to-mesenchymal transition (EMT) in scaffold culture of TNBC cells

The induction of EMT in human mammary epithelial cells is known to increase the BCSC subpopulation [17]. We therefore evaluated the expression of several transcription factors that execute EMT, such as *SNAIL*, *SLUG*, *ZEB1*, *ZEB2*, and *TWIST*, in 2D- and 3D-cultured cells. Proteins involved in this process, including E-cadherin and vimentin, were also analyzed to determine whether EMT was triggered during 3D culture and may be responsible of the stemness enrichment. In both cell models, *SNAIL* was found to be upregulated at early times of 3D cell culture (Fig. 4A and B). SNAIL is known to be a prominent EMT initiator since its expression was proven to be sufficient to induce EMT in primary breast cancer cells [83] and drug resistance [84]. Moreover, SNAIL expression was also associated with self-renewal through NANOG activation [85], which was upregulated in 3D-cultured MDA-MB-231 cells (Fig. 3A). SNAIL is known to bind to and represses its own promoter, indicating the existence of an autoregulatory loop [86]. This fact, along with its short half-life [87], proves the time-dependent trend showed in Fig. 4. In the basal-like cell model, *ZEB2* and *TWIST* were also overexpressed during 3D culture, with greater robustness after 6 days of incubation (Fig. 4B). We further measured gene and protein expression of E-cadherin (encoded by *CDH1*) and vimentin (encoded by *VIM*), the two major proteins involved in EMT (full Western blot membranes displayed in Table S5). 3D cell culture led to a downregulation on *CDH1* gene levels in both cell models (Fig. 4C and D). This fact resulted in a decrease of E-cadherin protein expression on the basal-like cells whereas expression in MDA-MB-231 model remained stable, probably because these cells are undergoing an early EMT. SNAIL, whose expression was upregulated in 3D culture (Fig. 4A and B), has been described as a direct repressor of E-cadherin through histone deacetylase activity [88]. Concerning vimentin, its gene expression was found upregulated when MDA-MB-231 cells were cultured on scaffolds for 6 days (Fig. 4C). An activation trend was described for protein analysis for both cell models as seen in Fig. 4C and D.

Considering these data, 3D cell culture with ES PCL scaffolds induced an EMT process to TNBC cells, which acquired a more invasive phenotype and led to an increase of the stemness features. Softness reported on PCL scaffolds could play a key role in this EMT induction, since it was proven to be an underlying mediator of TGF-β–driven processes such as EMT through dynamic compression and contraction of cell-matrix interaction [89]. Although the expression of structural proteins E-cadherin and vimentin were altered during scaffold culture, actin and tubulin levels, the main components of the eukaryotic cytoskeleton, were proven to be consistent among the different cell culture supports and incubation period for both cell lines (Fig. S2).

3.5. MAPK and PI3K/AKT/mTOR pathways modulation in scaffold-cultured TNBC cells

To discern whether cell metabolism is affected during 3D culture and stemness enrichment, MAPK and PI3K/AKT/mTOR pathways, which represent key mechanisms for cells to regulate cell survival, division, and motility, were characterized through Western blot (full membranes displayed in Table S5). MAPK pathway is involved in both physiological and pathological cell functions, including cell proliferation, differentiation, cell survival, oncogenesis, and tumor progression [90]. To evaluate the implication of the MAPK pathway in the stem-enriched 3D population, phosphorylated and total protein levels of MAPK, as well as the downstream phospho-S6, were analyzed (Fig. 5). Mesenchymal-like model MDA-MB-231 showed a pathway activation after 3 culture days within scaffolds, in accordance with the MAPK phosphorylated levels (Fig. 5A), which was not maintained at further culture times. On the other hand, basal-like MDA-MB-468 cell line displayed a clear downregulation of the MAPK pathway along time, even though total MAPK protein levels gradually increased during 3D culture (Fig. 5B). We hypothesized that increased activation level of MAPK at early times in MDA-MB-231 model was in part a response to cell cytoskeleton rearrangement on the PCL nanofibers. In fact, MAPK activation was related with cytoskeleton rearrangements in the same breast cancer model to increase the morphological plasticity for metastatic purposes [91]. For the other cell culture conditions, MAPK pathway, which regulates cell proliferation, seems downregulated in both TNBC cell lines possibly due to their lower cell growth rate in scaffolds as previously reported in the same 3D model [53,61]. Moreover, decreased MAPK signaling and activation of a quiescent profile have been related to decreased matrix stiffness, a condition found in the used ES PCL scaffolds compared to PS surfaces (Fig. 1) [92]. Phosphorylated levels of the MAPK-downstream S6 ribosomal protein were found not to be affected by 3D culture (Fig. 5). Therefore, differences on cell metabolism during scaffolds culture may be not mediated by p-S6, but probably by MAPK direct modulation of end-point effectors such as transcription factors.

The PI3K/AKT/mTOR signaling pathways play a key role in many physiological and pathological conditions, including cell proliferation, angiogenesis, metabolism, differentiation, and survival [93]. Interestingly, recent studies have demonstrated its importance in self-renew maintenance and tumorigenicity [94], EMT and radioresistance [95], mammosphere formation [96], and ALDH activity [97]. Therefore, the expression and activation of several proteins involved in the PI3K/AKT/mTOR cascade were analyzed (Fig. 5). MDA-MB-231 cells

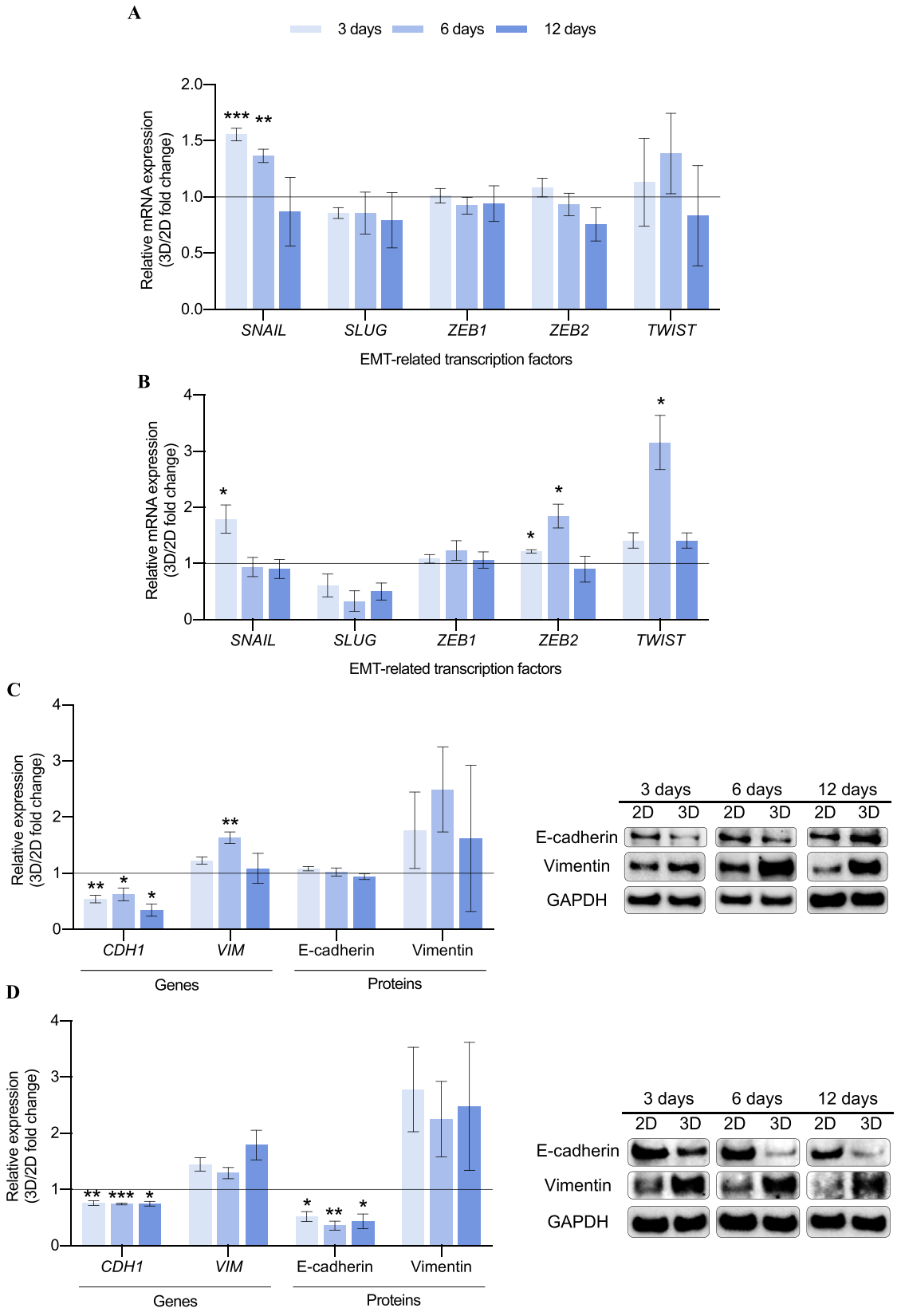

Fig. 4. Epithelial-to-mesenchymal transition (EMT) analysis for MDA-MB-231 (**A**, **C**) and MDA-MB-468 (**B**, **D**). Fold changes in mRNA levels of EMT-related genes (**A**, **B**) and in gene and protein expression of E-cadherin and vimentin (**C**, **D**) of cells cultured on ES PCL scaffolds (3D) compared to corresponding 2D control are depicted. Gene expression levels were quantified by double delta Ct analysis method. Both gene and protein expression levels were normalized against GAPDH values. Significant differences of 3D with regard to 2D cultures are indicated as * ($p < 0.05$), ** ($p < 0.01$) and *** ($p < 0.001$). A representative Western blot image for each cell culture condition is shown.

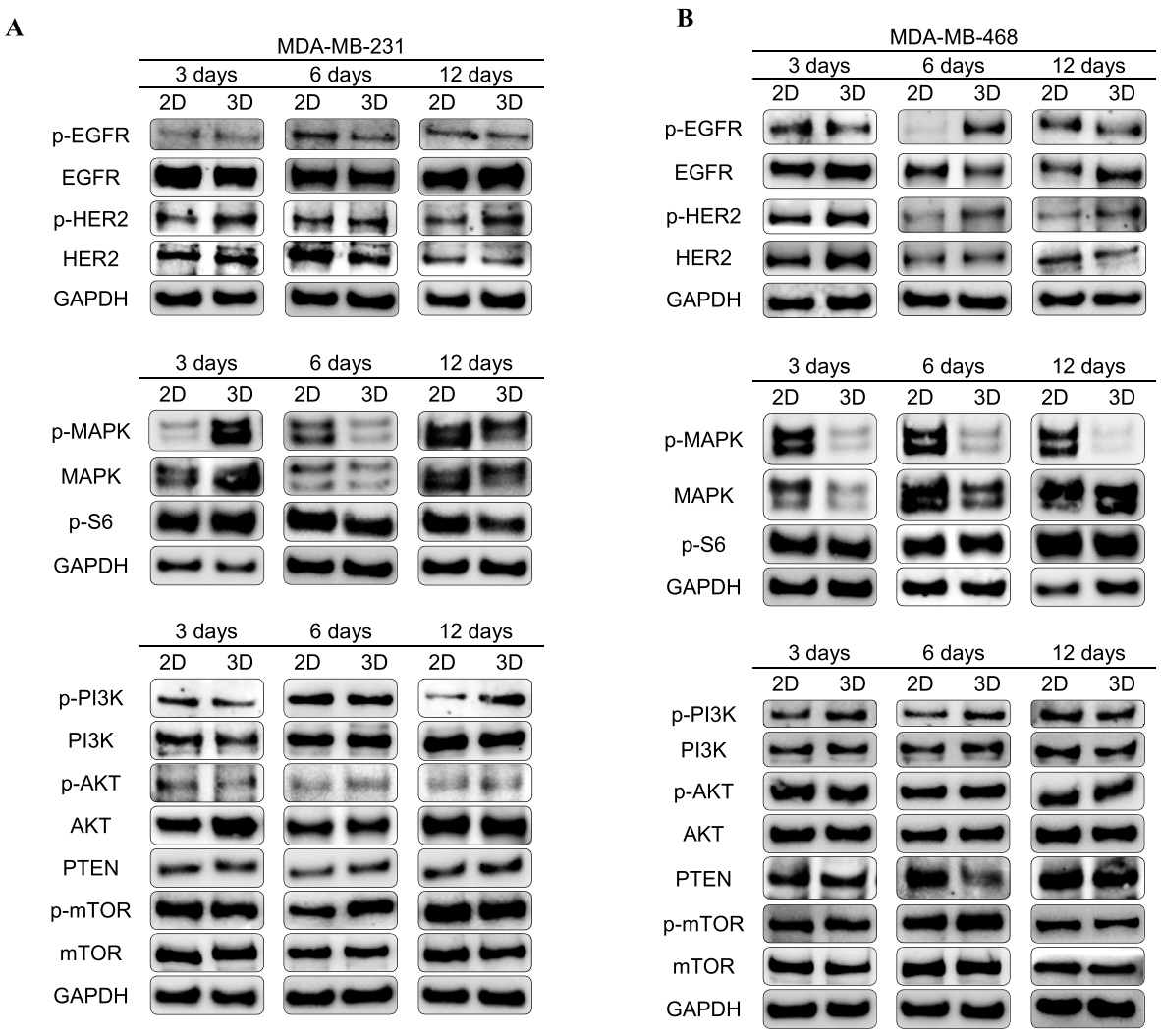

Fig. 5. Characterization of EGFR/HER2, MAPK and PI3K/AKT/mTOR pathways. Phosphorylation state and total protein levels were determined by Western blotting for MDA-MB-231 (**A**) and MDA-MB-468 (**B**) cells cultured on ES PCL scaffolds (3D) compared to corresponding 2D control. GAPDH was used as a control of protein loading. Results shown are representative of those obtained from 3 independent experiments.

showed an increasing activation of PI3K along 3D culture against the stable levels of total protein (Fig. 5A). This activation resulted in higher levels of total AKT protein and phosphorylated mTOR after 3 and 6 days of culture within scaffolds, respectively. Regarding the basal-like model MDA-MB-468, higher levels of activated PI3K and mTOR were found after 6 days of culture in scaffolds, accompanied by downregulation of PTEN, the negative regulator of the pathway (Fig. 5B). In the light of these results, 3D culture with ES PCL scaffolds led to a mild activation of the PI3K/AKT/mTOR pathway, as proved by the higher phosphorylation level of the downstream complex mTOR after 6 days of culture in both cell models.

In addition to their independent signaling programs, MAPK and PI3K/AKT/mTOR can either positively or negatively intraregulate [98,99]. For instance, in glioblastoma stem-like cells, inactivation of either MAPK or PI3K/mTOR pathway triggered activation of the other, suggesting a mutually inhibitory crosstalk between these two pathways [94]. Collectively, hyperactivation of PI3K/AKT/mTOR cascade may inhibit MAPK signaling, leading to a more quiescent culture. Or vice versa, cells adopted a less proliferative profile within 3D surroundings, leading to a MAPK inactivation and triggering PI3K/AKT/mTOR signaling due to a feedback loop. Contrary to our results, previous works pointed out that 3D culture of HER2+ breast cancer cells in Matrigel or spheres promoted a shift from PI3K/AKT to MAPK signaling [100–102]. Overall, this may indicate that cells can adopt different modifications upon 3D culture depending on their molecular subtype and 3D structure type, among other variables.

Not only are receptor tyrosine kinases critical regulators of several cell functions including proliferation, differentiation, and survival [103], but they also have a critical key role in cancer development and progression [104]. One of the most important receptors group is the ErbB/HER family, which includes the Epidermal Growth Factor Receptor (EGFR, also known as HER1) and the Human Epidermal growth factor Receptor 2 (HER2) [105]. The signal transduction caused by their activation promotes a diverse repertoire of cellular signaling pathways including MAPK or the PI3K/AKT/mTOR pathways [106]. As seen in Fig. 5A, MDA-MB-231 cells underwent a HER2 overexpression and activation after 3 days of culture in scaffolds. Alternatively, EGFR expression seemed stable, with a slight upregulation after 12 days of culture. About MDA-MB-468 cells, activation of EGFR and HER2 was observed after 6 days of culture in scaffolds (Fig. 5B). In addition, a previous study already reported overexpression of HER2 in breast and ovarian cancer cells following culture in 3D supports but not in 2D monolayers [100]. Activation of HER2 is associated with BCSCs and radioresistance in HER2-negative breast cancer cell models [107], as well as with tight junctions and cell polarity disruption [108].

Considering all these findings, our hypothesis is that upregulation of HER2 alone (MDA-MB-231) or in combination with that of EGFR (MDA-MB-468) may promote PI3K/AKT/mTOR activation during 3D cell culture, in detriment of MAPK signaling. These signaling alterations could be behind BCSC expansion within 3D culture, as PI3K pathway was previously related to the acquisition of CSC-like properties in breast cancer cells [109]. Besides, metabolism alterations were mainly found at 3 and 6 culture days, time points were BCSC took the greatest expansion in scaffolds. It is worth noting that HER2 is the preferred dimerization partner, since it possesses a conformation similar to a ligand-activated stated [110] and results in greater signal transduction compared with other family members [111]. Moreover, HER2 is thought to preferentially form homodimers in 3D suspension culture [100], proving its important role in both cell models. High levels of HER2 are speculated to promote spontaneous dimerization and causing constitutive HER2 activation and signaling [112].

3.6. Role of fatty acid synthase (FASN) enzyme in BCSC-enriched TNBC samples

3.6.1. FASN expression and activity on monolayer and 3D culture

Apart from the relation between stemness and FASN [39], HER2 is proven to stimulate FASN expression and post-translational activation by phosphorylation. FASN, in turn, contributes to HER2 activation allowing its incorporation in lipid rafts on the plasma membrane [113]. Therefore, gene and protein expression of FASN (encoded by *FASN*) was evaluated in 2D and 3D samples to discern a possible role of this enzyme during the acquisition of stemness features within scaffold culture (full Western blot membranes displayed in Table S5). As seen in Fig. 6A and B, *FASN* mRNA levels of both cell models were found slightly upregulated after 6 days of culture within PCL ES scaffolds. This moderate increase resulted in significantly higher protein levels at the aforementioned culture time. Note, FASN expression had the same trend in both cell models and it was found upregulated after 6 days of culture in scaffolds, the same incubation period which showed the maximum expansion of stemness features. For this reason, the enzyme activity of FASN was also evaluated after 6 days on monolayer or scaffold culture (Fig. 6C). Both cell models showed significantly greater FASN activity after their 3D culture. Therefore, either protein expression or functional FASN activity were determined to be upregulated in MDA-MB-231 and MDA-MB-468 cells following 6 days of culture within PCL meshes.

3.6.2. Pharmacological inhibition of FASN on monolayer and 3D culture

In the light of previous results, we wanted to investigate the impact of FASN inhibition on the BCSC-enriched population. Thus, TNBC cells were treated with the FASN inhibitors EGCG and G28 after 6 days of 2D or 3D culture, when both BCSC expansion and FASN hyperactivation took their maximum within scaffolds. Following a 48 h treatment, cell viability was assessed in both cell culture supports (Fig. 7A and B). Samples from 2D and 3D culture supports showed a similar behavior. There were no differences regarding inhibitory concentration between the tested TNBC cells cultured on 2D and 3D supports (Fig. S3). This data, contrary to the chemoresistance previously reported on 3D-cultured cells (Fig. 3C and D), opens the door to propose FASN as a novel target to treat 3D-cultured quiescent and stem-like TNBC populations.

To evaluate the effect on the BCSC niche, cells were treated with IC_{30} and IC_{50} values of EGCG and G28 (drug concentration that inhibited 30 or 50% of cell viability, respectively) in 2D- and 3D-cultured samples. IC values calculated with 2D-cultured cells were used since they are statistically similar to the ones from 3D samples (Fig. S3). After 48 h treatment, the capacity of forming mammospheres was evaluated as a marker of stem-like population. As seen in Fig. 7C and D, 3D-cultured samples showed significantly higher mammosphere forming capacity confirming the expansion of stemness features in untreated cells. The treatment with EGCG and G28 decreased the MFI values of 3D samples down to similar values of 2D or even lower. It should be noted that G28 exerted a greater impact upon the MDA-MB-231 model, in which 3D samples treated with IC_{50} dosage showed a significantly minor MFI value than the corresponding 2D control (Fig. 7C). On the other hand, basal-like MDA-MB-468 cells in scaffolds underwent a greater MFI decrease when treated with EGCG, also exhibiting an inferior mammosphere forming capacity than 2D cells (Fig. 7D). Taking all these findings into account, the

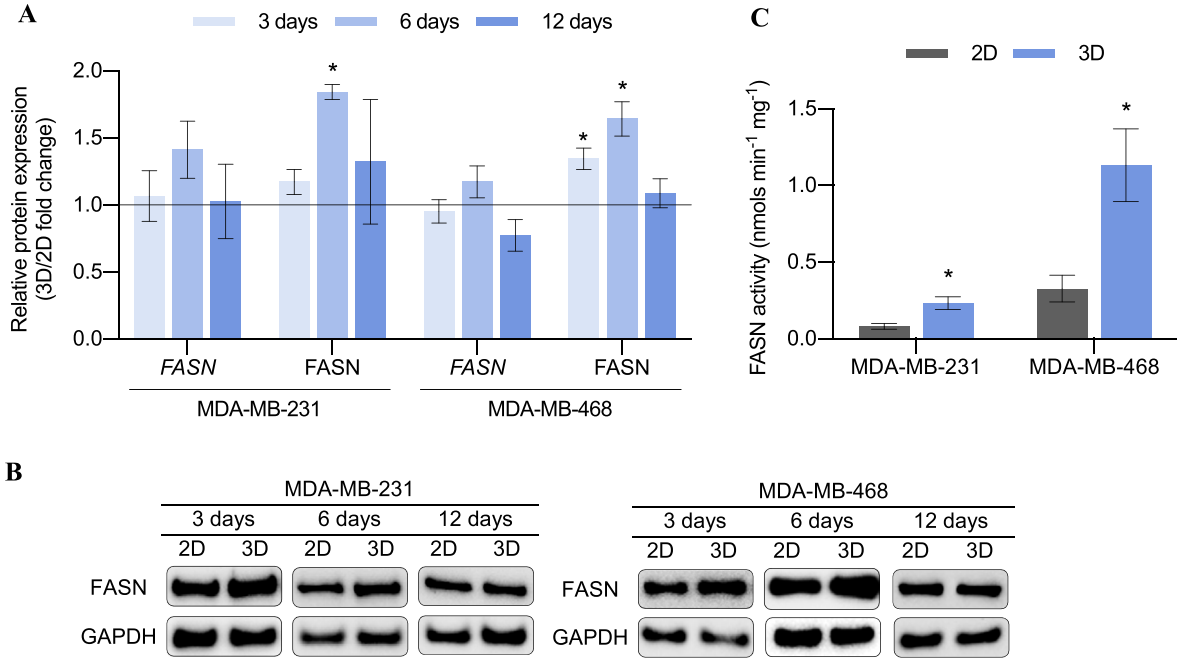

Fig. 6. FASN expression pattern. **(A)** Fold changes in gene and protein expression of FASN for MDA-MB-231 and MDA-MB-468 cells cultured on ES PCL scaffolds (3D) compared to corresponding 2D control. Gene expression levels were quantified by double delta Ct analysis method. Both gene and protein expression levels were normalized against GAPDH values. **(B)** A representative Western blot image for each cell culture condition is shown. **C** FASN activity analysis for MDA-MB-231 and MDA-MB-468 cells after 6 days of culture on monolayer (2D) and scaffolds (3D). Significant differences of 3D with regard to 2D cultures are indicated as * ($p < 0.05$).

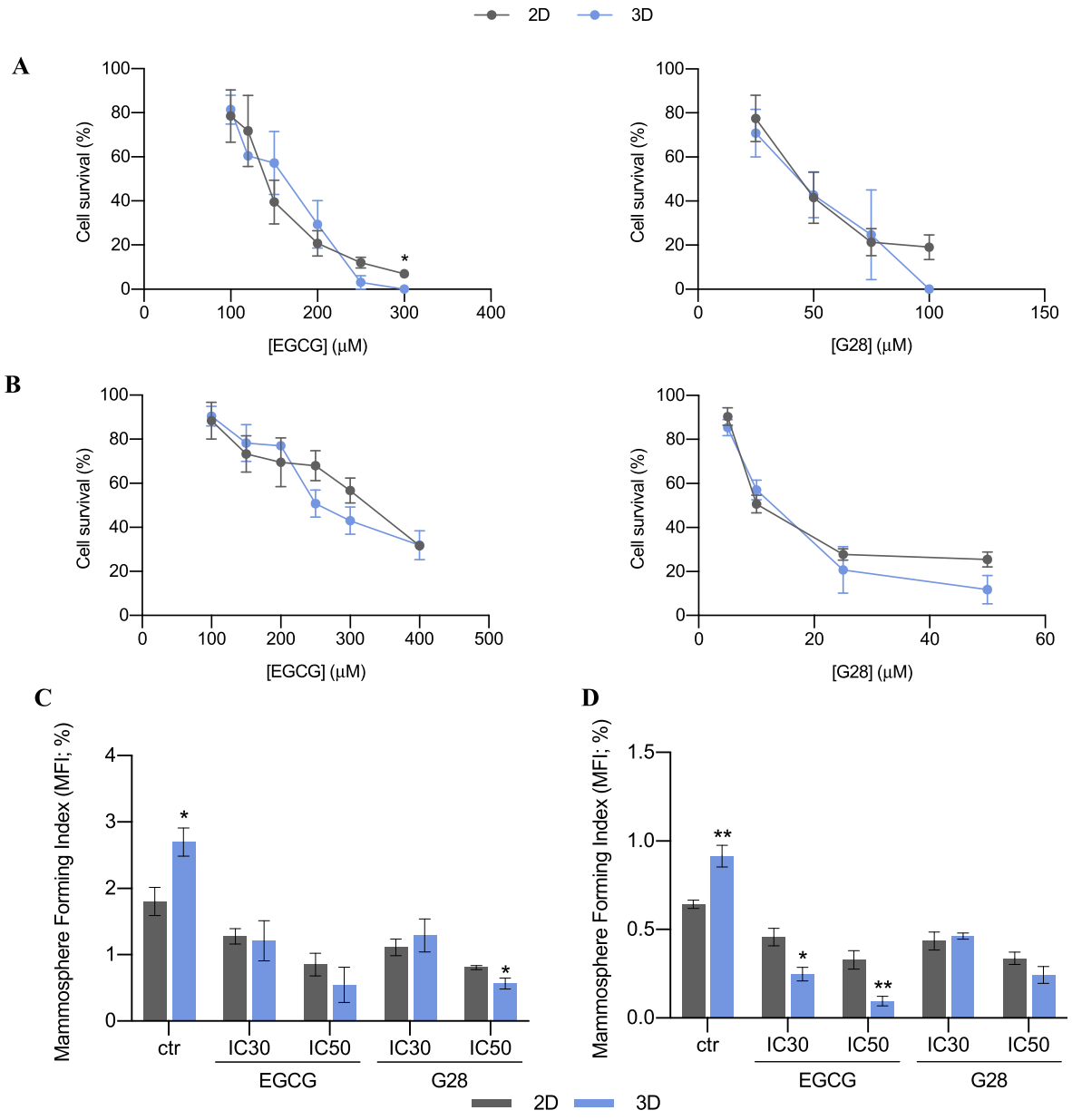

Fig. 7. Cell survival plots (**A**, **B**) and mammosphere forming assay (**C**, **D**) for MDA-MB-231 (**A**, **C**) and MDA-MB-468 (**B**, **D**) cells after EGCG or G28 treatment. Cells were cultured on monolayer (2D) or in PCL scaffolds (3D) for 6 days and then exposed to the FASN inhibitors EGCG and G28 for 48 h. Cell survival data are expressed as percentage of untreated cells as determined by MTT assay. IC_{30} and IC_{50} values were previously calculated from dose-response curves. Significant differences of 3D with regard to corresponding 2D cultures are indicated as * ($p < 0.05$) and ** ($p < 0.01$).

inhibition of FASN through EGCG and G28 treatment led to a stemness diminishment, overcoming the BCSC expansion achieved in 3D culture. In a similar fashion, resveratrol, a natural polyphenolic compound, has been proven to suppress tumor stem-like cells growth by inducing pro-apoptotic genes via downregulation of FASN expression, *in vitro* and with mice model [114]. Some authors pointed out a possible role of FASN increasing fatty acid levels during tumor cell migration, invasion, and metastasis, characteristics of the BCSC niche [115]. Despite this report and previous links between FASN and cancer stem-like cells, further investigations are needed to elucidate the mechanism through which stemness diminishes in response to FASN inhibition.

4. Conclusions

ES 15% PCL scaffolds used in the present work have been proven to provide a softer and more elastic 3D network compared with PS surfaces. As demonstrated in previous [53,61] and current research, 3D culture with this scaffold model led to an enrichment of the BCSC subpopulation in TNBC cells, resulting in higher mammosphere forming capacity, ALDH activity, $CD44^{+}/CD24^{-/low}$ cell proportion, stemness-related genes expression, and chemoresistance, specifically at early culture time points. In addition, EMT was revealed to occur throughout scaffold culture, which can transform epithelial cancer cells into cancer stem-like cells. Aside from BCSC expansion within scaffolds surroundings, 3D-cultured

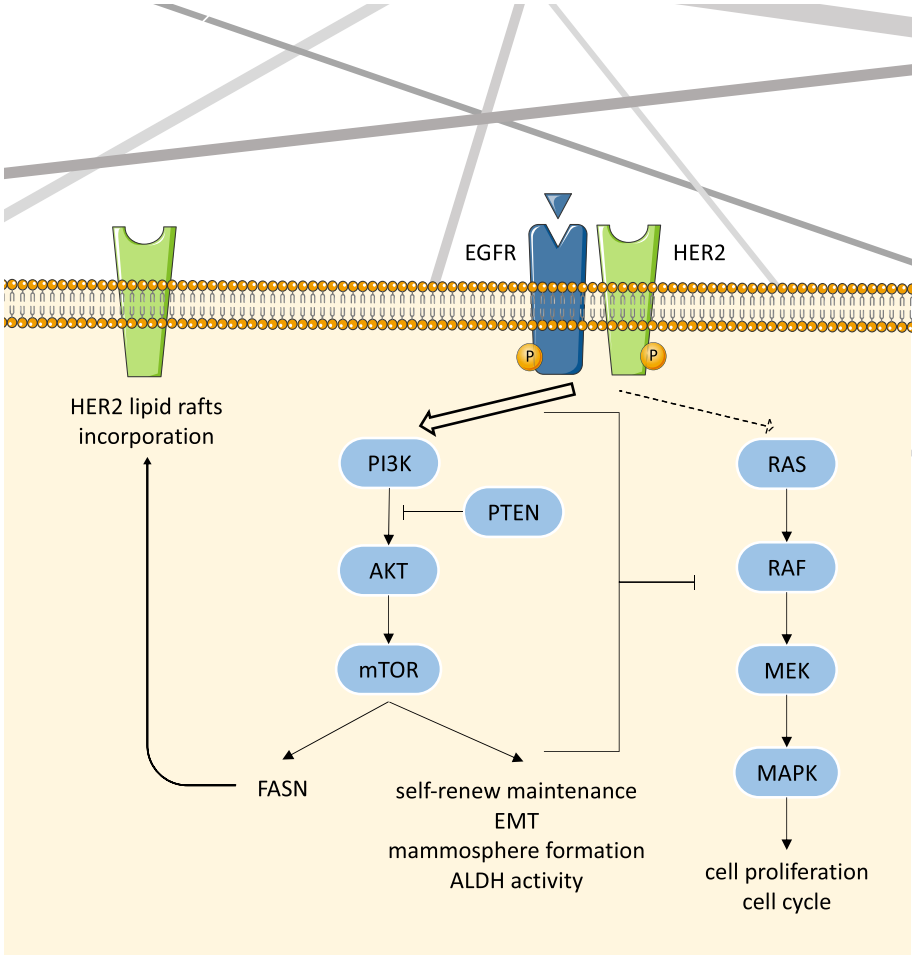

Fig. 8. Schematic representation of TNBC cell metabolism modulation within 3D ES PCL scaffold culture.

cells displayed a strong MAPK downregulation alongside a mild PI3K/AKT/mTOR activation, resulting in a quiescent cell profile and the upregulation of the aforementioned stemness features. As hypothesized in Fig. 8, this signaling switch may be modulated by the described activation of EGFR and HER2, which is proven to favor FASN synthesis, previously related to cancer cells and stemness. To the best of our knowledge, we are the first to define a FASN hyperactivation in stemness-enriched TNBC cells cultured on 3D structures. The addition of two FASN inhibitors led to a similar cell death in monolayer and scaffold-cultured cells, eluding the cell growth rate dependence of the chemoagents. Moreover, the inhibition of FASN overcame the BCSC enrichment achieved in 3D culture in terms of mammosphere forming capacity, suggesting the possibility to inhibit FASN to treat the cancer stem-like cells. However, more BCSC markers could be analyzed after FASN inhibition to confirm stemness diminishment, including ALDH activity and $CD44^{+}/CD24^{-/low}$ status.

Collectively, ES PCL scaffolds represent a potent tool to maintain the stemness features of the sample and expand the BCSC niche of TNBC cells by providing resemblance to a physiological structure. Nanofiber meshes may facilitate research in the cancer stem-like cell field, since novel biomarkers and treatments need to be developed to attack not only the bulk tumor, but also the quiescent and tumor-initiating cells. Notably, FASN deserves further investigation as a feasible biomarker for BCSC-enriched TNBC samples, specially within 3D surroundings. Despite the described links between FASN and stemness, more efforts would be needed to investigate whether BCSC expansion and signaling switch alongside FASN activation are two independent events occurred in a 3D environment, or there is a causal relation.

Author contributions

M.R., J.C., and T.P. conceived the ideas and designed the experiments. M.R. and E.P-A. performed the experiments and analysis. J.R. performed the FASN activity assay. M.Y. guided flow cytometry experiments and helped with statistical analysis. J.S-M. and A.M.K. guided CD44/CD24 experiments. M.P. and L.F. provided G28 drug. M.R., J.C., and T.P. wrote the manuscript. All authors discussed the study and commented on the manuscript.

Declaration of competing interest

The authors declare that they have no known competing financial interests or personal relationships that could have appeared to influence the work reported in this paper.

Acknowledgements

This work was supported by Spanish grants from Fundación Ramón Areces, Instituto de Salud Carlos III and co-funded by European Union (ERDF/ESF, “A way to make Europe”/”Investing in your future”) (PI19/00372), and Ministerio de Economía y Competitividad (DPI2016-77156-R). The authors are grateful to Marc Rabionet pre-doctoral grant (IFUdG2017/62), Emma Polonio-Alcalá pre-doctoral grant (2019FI_B01011), the support of the Catalan Government (2017SGR00385), and Oncolliga Foundation and RadikalSwim (OncoSwim). The authors thank the researcher Sabina Couto-Ovejero and the Research Technical Services from the University of Girona. The authors

are also grateful to Lynn Opdenaker and the flow cytometry core at the Cawley Center for Translational Research, Helen F Graham Cancer Center, which is supported by the Delaware INBRE program, with a grant from the National Institute of General Medical Sciences – NIGMS (P20 GM103446) from the National Institutes of Health and the State of Delaware.

Appendix A. Supplementary data

Supplementary data to this article can be found online at https://doi.org/10.1016/j.mtbio.2021.100155.

References

[1] J. Ferlay, M. Colombet, I. Soerjomataram, C. Mathers, D.M. Parkin, M. Piñeros, et al., Estimating the global cancer incidence and mortality in 2018: GLOBOCAN sources and methods, Int. J. Cancer 144 (2019) 1941–1953, https://doi.org/10.1002/ijc.31937.

[2] C.M. Perou, T. Sørlie, M.B. Eisen, M. van de Rijn, S.S. Jeffrey, C a Rees, et al., Molecular portraits of human breast tumours, Nature 406 (2000) 747–752, https://doi.org/10.1038/35021093.

[3] C.L. Griffiths, J.L. Olin, Triple negative breast cancer: a brief review of its characteristics and treatment options, J. Pharm. Pract. 25 (2012) 319–323, https://doi.org/10.1177/0897190012442062.

[4] S. S, B. S, S. Av, W. F, K.-S. M, I. Ec, et al., Triple negative breast cancers express receptors for LHRH and are potential therapeutic targets for cytotoxic LHRH-analogs, AEZS 108 and AEZS 125, BMC Cancer 14 (2014), https://doi.org/10.1186/1471-2407-14-847.

[5] J.D. Obayemi, A.A. Salifu, S.C. Eluu, V.O. Uzonwanne, S.M. Jusu, C.C. Nwazojie, et al., LHRH-conjugated drugs as targeted therapeutic agents for the specific targeting and localized treatment of triple negative breast cancer, Sci. Rep. 10 (2020 101 2020) 1–18, https://doi.org/10.1038/s41598-020-64979-1.

[6] K.R. Bauer, M. Brown, R.D. Cress, C.A. Parise, V. Caggiano, Descriptive analysis of estrogen receptor (ER)-negative, progesterone receptor (PR)-negative, and HER2-negative invasive breast cancer, the so-called triple-negative phenotype, Cancer 109 (2007) 1721–1728, https://doi.org/10.1002/cncr.22618.

[7] R. Dent, M. Trudeau, K.I. Pritchard, W.M. Hanna, H.K. Kahn, C.A. Sawka, et al., Triple-negative breast cancer: clinical features and patterns of recurrence, Clin. Cancer Res. 13 (2007).

[8] L.A. Carey, E.C. Dees, L. Sawyer, L. Gatti, D.T. Moore, F. Collichio, et al., The triple negative paradox: primary tumor chemosensitivity of breast cancer subtypes, Clin. Cancer Res. 13 (2007) 2329–2334, https://doi.org/10.1158/1078-0432.CCR-06-1109.

[9] A. Prat, J.S. Parker, O. Karginova, C. Fan, C. Livasy, J.I. Herschkowitz, et al., Phenotypic and molecular characterization of the claudin-low intrinsic subtype of breast cancer, Breast Cancer Res. 12 (2010), https://doi.org/10.1186/bcr2635.

[10] M. Diehn, R.W. Cho, N.A. Lobo, T. Kalisky, M.J. Dorie, A.N. Kulp, et al., Association of reactive oxygen species levels and radioresistance in cancer stem cells, Nature 458 (2009) 780–783, https://doi.org/10.1038/nature07733.

[11] X. Zhang, K. Powell, L. Li, Breast cancer stem cells: biomarkers, identification and isolation methods, regulating mechanisms, cellular origin, and beyond, Cancers 12 (2020) 1–28, https://doi.org/10.3390/cancers12123765.

[12] F.L. Shaw, H. Harrison, K. Spence, M.P. Ablett, B.M. Simões, G. Farnie, et al., A detailed mammosphere assay protocol for the quantification of breast stem cell activity, J. Mammary Gland Biol. Neoplasia 17 (2012) 111–117, https://doi.org/10.1007/s10911-012-9255-3.

[13] C. Ginestier, M.H. Hur, E. Charafe-Jauffret, F. Monville, J. Dutcher, M. Brown, et al., ALDH1 is a marker of normal and malignant human mammary stem cells and a predictor of poor clinical outcome, Cell Stem Cell 1 (2007) 555–567, https://doi.org/10.1016/j.stem.2007.08.014.

[14] M. Al-Hajj, M.S. Wicha, A. Benito-Hernandez, S.J. Morrison, M.F. Clarke, Prospective identification of tumorigenic breast cancer cells, Proc. Natl. Acad. Sci. U. S. A. 100 (2003) 3983–3988, https://doi.org/10.1073/pnas.0530291100.

[15] B.G. Hollier, K. Evans, S.A. Mani, The epithelial-to-mesenchymal transition and cancer stem cells: a coalition against cancer therapies, J. Mammary Gland Biol. Neoplasia 14 (2009) 29–43, https://doi.org/10.1007/s10911-009-9110-3.

[16] S.A. Mani, W. Guo, M.-J. Liao, E.N. Eaton, A. Ayyanan, A.Y. Zhou, et al., The epithelial-mesenchymal transition generates cells with properties of stem cells, Cell 133 (2008) 704–715, https://doi.org/10.1016/j.cell.2008.03.027.

[17] A.-P. Morel, M. Lièvre, C. Thomas, G. Hinkal, S. Ansieau, A. Puisieux, Generation of breast cancer stem cells through epithelial-mesenchymal transition, PLoS One 3 (2008) e2888, https://doi.org/10.1371/journal.pone.0002888.

[18] J.J. Christiansen, A.K. Rajasekaran, Reassessing epithelial to mesenchymal transition as a prerequisite for carcinoma invasion and metastasis, Cancer Res. 66 (2006) 8319–8326, https://doi.org/10.1158/0008-5472.CAN-06-0410.

[19] C.Y. Liu, H.H. Lin, M.J. Tang, Y.K. Wang, Vimentin contributes to epithelial-mesenchymal transition cancer cell mechanics by mediating cytoskeletal organization and focal adhesion maturation, Oncotarget 6 (2015) 15966–15983, https://doi.org/10.18632/oncotarget.3862.

[20] H.S. Sul, D. Wang, Nutritional and hormonal regulation of enzymes in fat synthesis: studies of fatty acid synthase and mitochondrial glycerol-3-phosphate acyltransferase gene transcription, Annu. Rev. Nutr. 18 (1998) 331–351, https://doi.org/10.1146/annurev.nutr.18.1.331.

[21] S.M. Anderson, M.C. Rudolph, J.L. McManaman, M.C. Neville, Key stages in mammary gland development. Secretory activation in the mammary gland: it's not just about milk protein synthesis, Breast Cancer Res. 9 (2007) 204, https://doi.org/10.1186/bcr1653.

[22] F.P. Kuhajda, Fatty-acid synthase and human cancer: new perspectives on its role in tumor biology, Nutrition 16 (2000) 202–208, https://doi.org/10.1016/S0899-9007(99)00266-X.

[23] S.F. Jones, J.R. Infante, Molecular pathways: fatty acid synthase, Clin. Cancer Res. 21 (2015) 5434–5438, https://doi.org/10.1158/1078-0432.CCR-15-0126.

[24] S. Bandyopadhyay, R. Zhan, Y. Wang, S.K. Pai, S. Hirota, S. Hosobe, et al., Mechanism of apoptosis induced by the inhibition of fatty acid synthase in breast cancer cells, Cancer Res. 66 (2006) 5934–5940, https://doi.org/10.1158/0008-5472.CAN-05-3197.

[25] T. Puig, A. Vázquez-Martín, J. Relat, J. Pétriz, J.A. Menéndez, R. Porta, et al., Fatty acid metabolism in breast cancer cells: differential inhibitory effects of epigallocatechin gallate (EGCG) and C75, Breast Cancer Res. Treat. 109 (2008) 471–479, https://doi.org/10.1007/s10549-007-9678-5.

[26] A. Blancafort, A. Giró-Perafita, G. Oliveras, S. Palomeras, C. Turrado, Campuzano Ò, et al., Dual fatty acid synthase and HER2 signaling blockade shows marked antitumor activity against breast cancer models resistant to Anti-HER2 drugs, PLoS One 10 (2015), https://doi.org/10.1371/journal.pone.0131241.

[27] E. Rysman, K. Brusselmans, K. Scheys, L. Timmermans, R. Derua, S. Munck, et al., De novo lipogenesis protects cancer cells from free radicals and chemotherapeutics by promoting membrane lipid saturation, Cancer Res. 70 (2010) 8117–8126, https://doi.org/10.1158/0008-5472.CAN-09-3871.

[28] A.S. Meena, A. Sharma, R. Kumari, N. Mohammad, S.V. Singh, M.K. Bhat, Inherent and acquired resistance to paclitaxel in hepatocellular carcinoma: molecular events involved, PLoS One 8 (2013), e61524, https://doi.org/10.1371/journal.pone.0061524.

[29] R. Ventura, K. Mordec, J. Waszczuk, Z. Wang, J. Lai, M. Fridlib, et al., Inhibition of de novo Palmitate Synthesis by Fatty Acid Synthase Induces Apoptosis in Tumor Cells by Remodeling Cell Membranes, Inhibiting Signaling Pathways, and Reprogramming Gene Expression, EBioMedicine 2 (2015) 808–824, https://doi.org/10.1016/j.ebiom.2015.06.020.

[30] X. Wang, W. Tian, Green tea epigallocatechin gallate: a natural inhibitor of fatty-acid synthase, Biochem. Biophys. Res. Commun. 288 (2001) 1200–1206, https://doi.org/10.1006/bbrc.2001.5923.

[31] D. Chen, S.B. Wan, H. Yang, J. Yuan, T.H. Chan, Q.P. Dou, EGCG, green tea polyphenols and their synthetic analogs and prodrugs for human cancer prevention and treatment, Adv. Clin. Chem. 53 (2011), https://doi.org/10.1016/B978-0-12-385855-9.00007-2.

[32] T. Puig, H. Aguilar, S. Cufí, G. Oliveras, C. Turrado, S. Ortega-Gutiérrez, et al., A novel inhibitor of fatty acid synthase shows activity against HER2+ breast cancer xenografts and is active in anti-HER2 drug-resistant cell lines, Breast Cancer Res. 13 (2011) R131, https://doi.org/10.1186/bcr3077.

[33] J. Crous-Masó, S. Palomeras, J. Relat, C. Camó, Martínez-Garza Ú, M. Planas, et al., (−)-Epigallocatechin 3-gallate synthetic analogues inhibit fatty acid synthase and show anticancer activity in triple negative breast cancer, Molecules 23 (2018), https://doi.org/10.3390/molecules23051160.

[34] A. Vazquez-Martin, B. Corominas-Faja, S. Cufi, L. Vellon, C. Oliveras-Ferraros, O.J. Menendez, et al., The mitochondrial H+-ATP synthase and the lipogenic switch New core components of metabolic reprogramming in induced pluripotent stem (iPS) cells, Cell Cycle 12 (2013) 207–218, https://doi.org/10.4161/cc.23352.

[35] Y. Yasumoto, H. Miyazaki, L.K. Vaidyan, Y. Kagawa, M. Ebrahimi, Y. Yamamoto, et al., Inhibition of fatty acid synthase decreases expression of stemness markers in glioma stem cells, PLoS One 11 (2016) 1–14, https://doi.org/10.1371/journal.pone.0147717.

[36] P.R. Pandey, H. Okuda, M. Watabe, S.K. Pai, W. Liu, a Kobayashi, et al., Resveratrol suppresses growth of cancer stem-like cells by inhibiting fatty acid synthase, Breast Cancer Res. Treat. 130 (2011) 387–398, https://doi.org/10.1007/s10549-010-1300-6.

[37] A.M. Gonzalez-Guerrico, I. Espinoza, B. Schroeder, C.H. Park, C.M. Kvp, A. Khurana, et al., Suppression of endogenous lipogenesis induces reversion of the malignant phenotype and normalized differentiation in breast cancer, Oncotarget (2016), https://doi.org/10.18632/oncotarget.9463.

[38] A. Giró-Perafita, M. Rabionet, M. Planas, L. Feliu, J. Ciurana, S. Ruiz-Martínez, et al., EGCG-derivative G28 shows high efficacy inhibiting the mammosphere-forming capacity of sensitive and resistant TNBC models, Molecules 24 (2019) 1027, https://doi.org/10.3390/molecules24061027.

[39] H. Li, Z. Feng, M.L. He, Lipid metabolism alteration contributes to and maintains the properties of cancer stem cells, Theranostics 10 (2020) 7053–7069, https://doi.org/10.7150/thno.41388.

[40] E. Charafe-Jauffret, C. Ginestier, F. Iovino, J. Wicinski, N. Cervera, P. Finetti, et al., Breast cancer cell lines contain functional cancer stem cells with metastatic capacity and a distinct molecular signature, Cancer Res. 69 (2009) 1302–1313, https://doi.org/10.1158/0008-5472.CAN-08-2741.

[41] A. Tsuyada, A. Chow, J. Wu, G. Somlo, P. Chu, S. Loera, et al., CCL2 mediates cross-talk between cancer cells and stromal fibroblasts that regulates breast cancer stem cells, Cancer Res. 72 (2012) 2768–2779, https://doi.org/10.1158/0008-5472.CAN-11-3567.

[42] C.H. Thomas, J.H. Collier, C.S. Sfeir, K.E. Healy, Engineering gene expression and protein synthesis by modulation of nuclear shape, Proc. Natl. Acad. Sci. U. S. A. 99 (2002) 1972–1977, https://doi.org/10.1073/pnas.032668799.

[43] L. Vergani, M. Grattarola, C. Nicolini, Modifications of chromatin structure and gene expression following induced alterations of cellular shape, Int. J. Biochem. Cell Biol. 36 (2004) 1447–1461, https://doi.org/10.1016/j.biocel.2003.11.015.

[44] G. Bao, S. Suresh, Cell and molecular mechanics of biological materials, Nat. Mater. 2 (2003) 715–725, https://doi.org/10.1038/nmat1001.

[45] C.-M. Lo, H.-B. Wang, M. Dembo, Y.-L. Wang, Cell Movement Is Guided by the Rigidity of the Substrate, 2000.

[46] T. Yeung, P.C. Georges, L.A. Flanagan, B. Marg, M. Ortiz, M. Funaki, et al., Effects of substrate stiffness on cell morphology, cytoskeletal structure, and adhesion, Cell Motil Cytoskeleton 60 (2005) 24–34, https://doi.org/10.1002/cm.20041.

[47] E. Jabbari, S.K. Sarvestani, L. Daneshian, S. Moeinzadeh, Optimum 3D matrix stiffness for maintenance of cancer stem cells is dependent on tissue origin of cancer cells, PLoS One 10 (2015), e0132377, https://doi.org/10.1371/JOURNAL.PONE.0132377.

[48] Y. Li, R. Randriantsilefisoa, J. Chen, J.L. Cuellar-Camacho, W. Liang, W. Li, Matrix stiffness regulates chemosensitivity, stemness characteristics, and autophagy in breast cancer cells, ACS Appl Bio Mater 3 (2020) 4474–4485, https://doi.org/10.1021/ACSABM.0C00448.

[49] E. Knight, S. Przyborski, Advances in 3D cell culture technologies enabling tissue-like structures to be created in vitro, J. Anat. 1–11 (2014), https://doi.org/10.1111/joa.12257.

[50] M. Chen, P.K. Patra, S.B. Warner, S. Bhowmick, Optimization of electrospinning process parameters for tissue engineering scaffolds, Biophys. Rev. Lett. 1 (2006) 153–178, https://doi.org/10.1142/S1793048006000148.

[51] L.A. Bosworth, S. Downes, Acetone, a sustainable solvent for electrospinning poly(ε-caprolactone) fibres: effect of varying parameters and solution concentrations on fibre diameter, J. Polym. Environ. 20 (2012) 879–886, https://doi.org/10.1007/s10924-012-0436-3.

[52] M.A. Woodruff, D.W. Hutmacher, The return of a forgotten polymer - polycaprolactone in the 21st century, Prog. Polym. Sci. 35 (2010) 1217–1256, https://doi.org/10.1016/j.progpolymsci.2010.04.002.

[53] M. Rabionet, M. Yeste, T. Puig, J. Ciurana, Electrospinning PCL scaffolds manufacture for three-dimensional breast cancer cell culture, Polymers 9 (2017) 328, https://doi.org/10.3390/polym9080328.

[54] S. Saha, X. Duan, L. Wu, P.-K. Lo, H. Chen, Q. Wang, Electrospun fibrous scaffolds promote breast cancer cell alignment and epithelial-mesenchymal transition, Langmuir 28 (2012) 2028–2034, https://doi.org/10.1021/la203846w.

[55] S. Feng, X. Duan, P.-K. Lo, S. Liu, X. Liu, H. Chen, et al., Expansion of breast cancer stem cells with fibrous scaffolds, Integr Biol (Camb) 5 (2013) 768–777, https://doi.org/10.1039/c3ib20255k.

[56] J. Sims-Mourtada, R.a. Niamat, S. Samuel, C. Eskridge, E.B. Kmiec, Enrichment of breast cancer stem-like cells by growth on electrospun polycaprolactone-chitosan nanofiber scaffolds, Int. J. Nanomed. 9 (2014) 995–1003, https://doi.org/10.2147/IJN.S55720.

[57] M. Rabionet, T. Puig, J. Ciurana, Electrospinning parameters selection to manufacture polycaprolactone scaffolds for three-dimensional breast cancer cell culture and enrichment, Procedia CIRP 65 (2017) 267–272, https://doi.org/10.1016/j.procir.2017.03.341.

[58] P. Russo, D. Acierno, A. Corradi, C. Leonelli, Dynamic-mechanical behavior and morphology of polystyrene/perovskite composites: effects of filler size, in: Procedia Eng., vol. 10, Elsevier, 2011, pp. 1017–1022, https://doi.org/10.1016/j.proeng.2011.04.167.

[59] M. Worzakowska, Thermal and mechanical properties of polystyrene modified with esters derivatives of 3-phenylprop-2-en-1-ol, J. Therm. Anal. Calorim. 121 (2015) 235–243, https://doi.org/10.1007/s10973-015-4547-7.

[60] A. Samani, J. Zubovits, D. Plewes, Elastic moduli of normal and pathological human breast tissues: an inversion-technique-based investigation of 169 samples, Phys. Med. Biol. 52 (2007) 1565–1576, https://doi.org/10.1088/0031-9155/52/6/002.

[61] M. Rabionet, T. Puig, J. Ciurana, Manufacture of PCL scaffolds through electrospinning technology to accommodate triple negative breast cancer cells culture, Procedia CIRP 89 (2020) 98–103.

[62] A.L. Jones R, Soft Condensed Matter, 2002.

[63] L. McKeen, Renewable Resource and Biodegradable Polymers. Eff. Steriliz. Plast. Elastomers, Elsevier, 2012, pp. 305–317, https://doi.org/10.1016/b978-1-4557-2598-4.00012-5.

[64] S. Tiptipakorn, N. Keungputpong, S. Phothiphiphit, S. Rimdusit, Effects of polycaprolactone molecular weights on thermal and mechanical properties of polybenzoxazine, J. Appl. Polym. Sci. 132 (2015), https://doi.org/10.1002/app.41915 n/a-n/a.

[65] D. Priselac, T. Tomašegović, THERMAL, surface and mechanical properties OF pcl/pla composites with coconut fibres as an alternative material to photopolymer printing plates, Teh Glas 11 (2017) 111–116.

[66] J. Rieger, The glass transition temperature of polystyrene. Results of a round robin test, J. Therm. Anal. 46 (1996) 965–972, https://doi.org/10.1007/BF01983614.

[67] S. Schindelmann, J. Windisch, R. Grundmann, R. Kreienberg, R. Zeillinger, H. Deissler, Expression profiling of mammary carcinoma cell lines: correlation of in vitro invasiveness with expression of CD24, Tumor Biol. 23 (2002) 139–145, https://doi.org/10.1159/000064030.

[68] S. Okumura-Nakanishi, M. Saito, H. Niwa, F. Ishikawa, Oct-3/4 and Sox2 regulate *oct-3/4* gene in embryonic stem cells, J. Biol. Chem. 280 (2005) 5307–5317, https://doi.org/10.1074/jbc.M410015200.

[69] N. Yang, Y. Wang, L. Hui, X. Li, X. Jiang, Silencing SOX2 expression by RNA interference inhibits proliferation, invasion and metastasis, and induces apoptosis through MAP4K4/JNK signaling pathway in human laryngeal cancer TU212 cells, J. Histochem. Cytochem. 63 (2015) 721–733, https://doi.org/10.1369/0022155415590829.

[70] A.I. Penzo-Méndez, Critical roles for SoxC transcription factors in development and cancer, Int. J. Biochem. Cell Biol. 42 (2010) 425–428, https://doi.org/10.1016/j.biocel.2009.07.018.Critical.

[71] D.J. Rodda, J.L. Chew, L.H. Lim, Y.H. Loh, B. Wang, H.H. Ng, et al., Transcriptional regulation of nanog by OCT4 and SOX2, J. Biol. Chem. 280 (2005) 24731–24737, https://doi.org/10.1074/jbc.M502573200.

[72] K.R. Yu, S.R. Yang, J.W. Jung, H. Kim, K. Ko, D.W. Han, et al., CD49f enhances multipotency and maintains stemness through the direct regulation of OCT4 and SOX2, Stem Cell. 30 (2012) 876–887, https://doi.org/10.1002/stem.1052.

[73] O. Leis, A. Eguiara, E. Lopez-Arribillaga, M.J. Alberdi, S. Hernandez-Garcia, K. Elorriaga, et al., Sox2 expression in breast tumours and activation in breast cancer stem cells, Oncogene 31 (2012) 1354–1365, https://doi.org/10.1038/onc.2011.338.

[74] J. Zhang, Q. Liang, Y. Lei, M. Yao, L. Li, X. Gao, et al., SOX4 induces epithelial-mesenchymal transition and contributes to breast cancer progression, Cancer Res. 72 (2012) 4597–4608, https://doi.org/10.1158/0008-5472.CAN-12-1045.

[75] X. Li, M.T. Lewis, J. Huang, C. Gutierrez, C.K. Osborne, M.-F. Wu, et al., Intrinsic resistance of tumorigenic breast cancer cells to chemotherapy, JNCI J Natl Cancer Inst 100 (2008) 672–679, https://doi.org/10.1093/jnci/djn123.

[76] M.D. Kars, G. Yıldırım, Determination of the target proteins in chemotherapy resistant breast cancer stem cell-like cells by protein array, Eur. J. Pharmacol. 848 (2019) 23–29, https://doi.org/10.1016/j.ejphar.2019.01.052.

[77] L.A. Quayle, P.D. Ottewell, I. Holen, Chemotherapy resistance and stemness in mitotically quiescent human breast cancer cells identified by fluorescent dye retention, Clin. Exp. Metastasis 35 (2018) 831–846, https://doi.org/10.1007/s10585-018-9946-2.

[78] J. Mehanna, F.G.H. Haddad, R. Eid, M. Lambertini, H.R. Kourie, Triple-negative breast cancer: current perspective on the evolving therapeutic landscape, Int J Womens Health 11 (2019) 431–437, https://doi.org/10.2147/IJWH.S178349.

[79] P. Mukherjee, A. Gupta, D. Chattopadhyay, U. Chatterji, Modulation of SOX2 expression delineates an end-point for paclitaxel-effectiveness in breast cancer stem cells, Sci. Rep. 7 (2017) 1–16, https://doi.org/10.1038/s41598-017-08971-2.

[80] A.-K. L, K.K. A B, F. At, B. Se, Targeting MDR in breast and lung cancer: discriminating its potential importance from the failure of drug resistance reversal studies, Drug Resist. Updates 15 (2012) 50–61, https://doi.org/10.1016/J.DRUP.2012.02.002.

[81] C. S, E. J, O.E. M E-S, Breast cancer chemoresistance: emerging importance of cancer stem cells, Surg Oncol 19 (2010) 27–32, https://doi.org/10.1016/J.SURONC.2009.01.004.

[82] C.-H. Choi, ABC transporters as multidrug resistance mechanisms and the development of chemosensitizers for their reversal, Cancer Cell Int. 5 (2005) 30, https://doi.org/10.1186/1475-2867-5-30.

[83] S.E. Moody, D. Perez, T.C. Pan, C.J. Sarkisian, C.P. Portocarrero, C.J. Sterner, et al., The transcriptional repressor Snail promotes mammary tumor recurrence, Cancer Cell 8 (2005) 197–209, https://doi.org/10.1016/j.ccr.2005.07.009.

[84] W. Li, C. Liu, Y. Tang, H. Li, F. Zhou, S. Lv, Overexpression of snail accelerates adriamycin induction of multidrug resistance in breast cancer cells, Asian Pac. J. Cancer Prev. APJCP 12 (2011) 2575–2580.

[85] C.W. Liu, C.H. Li, Y.J. Peng, Y.W. Cheng, H.W. Chen, P.L. Liao, et al., Snail regulates Nanog status during the epithelial-mesenchymal transition via the Smad1/Akt/GSK3β signaling pathway in non-small-cell lung cancer, Oncotarget 5 (2014) 3880–3894, https://doi.org/10.18632/oncotarget.2006.

[86] S. Peiró, M. Escrivà, I. Puig, M.J. Barberà, N. Dave, N. Herranz, et al., Snail1 transcriptional repressor binds to its own promoter and controls its expression, Nucleic Acids Res. 34 (2006) 2077–2084, https://doi.org/10.1093/nar/gkl141.

[87] Y. Wang, J. Shi, K. Chai, X. Ying, B. Zhou, The role of snail in EMT and tumorigenesis, Curr. Cancer Drug Targets 13 (2014) 963–972, https://doi.org/10.2174/15680096113136660102.

[88] H. Peinado, E. Ballestar, M. Esteller, A. Cano, Snail mediates E-cadherin repression by the recruitment of the Sin3A/histone deacetylase 1 (HDAC1)/HDAC2 complex, Mol. Cell Biol. 24 (2004) 306–319, https://doi.org/10.1128/MCB.24.1.306.

[89] R.G. Wells, D.E. Discher, Matrix elasticity, cytoskeletal tension, and TGF-β : the insoluble and soluble meet, Sci. Signal. 1 (2008) pe13, https://doi.org/10.1126/stke.110pe13.

[90] G. Pearson, F. Robinson, T.B. Gibson, B.-E. Xu, M. Karandikar, K. Berman, et al., Mitogen-activated protein (MAPK) kinase pathways: regulation and physiological functions, Endocr. Rev. 22 (2001) 153–183, https://doi.org/10.1016/S0955-0674(97)80061-0.

[91] D.A. Rudzka, G. Spennati, D.J. McGarry, Y.H. Chim, M. Neilson, A. Ptak, et al., Migration through physical constraints is enabled by MAPK-induced cell softening via actin cytoskeleton re-organization, J. Cell Sci. 132 (2019), https://doi.org/10.1242/jcs.224071.

[92] P.P. Provenzano, D.R. Inman, K.W. Eliceiri, P.J. Keely, Matrix density-induced mechanoregulation of breast cell phenotype, signaling and gene expression through a FAK-ERK linkage, Oncogene 28 (2009) 4326–4343, https://doi.org/10.1038/onc.2009.299.

[93] C. Porta, C. Paglino, A. Mosca, Targeting PI3K/Akt/mTOR signaling in cancer, Front Oncol 4 APR (2014), https://doi.org/10.3389/fonc.2014.00064.

[94] J. Sunayama, K.I. Matsuda, A. Sato, K. Tachibana, K. Suzuki, Y. Narita, et al., Crosstalk between the PI3K/mTOR and MEK/ERK pathways involved in the maintenance of self-renewal and tumorigenicity of glioblastoma stem-like cells, Stem Cell. 28 (2010) 1930–1939, https://doi.org/10.1002/stem.521.

[95] L. Chang, P.H. Graham, J. Hao, J. Ni, J. Bucci, P.J. Cozzi, et al., Acquisition of epithelialmesenchymal transition and cancer stem cell phenotypes is associated with activation of the PI3K/Akt/mTOR pathway in prostate cancer radioresistance, Cell Death Dis. 4 (2013), https://doi.org/10.1038/cddis.2013.407.

[96] J. Zhou, J. Wulfkuhle, H. Zhang, P. Gu, Y. Yang, J. Deng, et al., Activation of the PTEN/mTOR/STAT3 pathway in breast cancer stem-like cells is required for viability and maintenance, Proc. Natl. Acad. Sci. U. S. A. 104 (2007) 16158–16163, https://doi.org/10.1073/pnas.0702596104.

[97] W.W. Chang, R.J. Lin, J. Yu, W.Y. Chang, C.H. Fu, A.C.Y. Lai, et al., The expression and significance of insulin-like growth factor-1 receptor and its pathway on breast cancer stem/progenitors, Breast Cancer Res. 15 (2013), https://doi.org/10.1186/bcr3423.

[98] J. Sunayama, K.-I. Matsuda, A. Sato, K. Tachibana, K. Suzuki, Y. Narita, et al., Crosstalk between the PI3K/mTOR and MEK/ERK pathways involved in the maintenance of self-renewal and tumorigenicity of glioblastoma stem-like cells, Stem Cell. 28 (2010) 1930–1939, https://doi.org/10.1002/stem.521.

[99] M.C. Mendoza, E. Emrah Er, J. Blenis, The Ras-ERK and PI3K-mTOR Pathways: Cross-Talk and Compensation, 2011, https://doi.org/10.1016/j.tibs.2011.03.006.

[100] M. Pickl, C.H. Ries, Comparison of 3D and 2D tumor models reveals enhanced HER2 activation in 3D associated with an increased response to trastuzumab, Oncogene 28 (2009) 461–468, https://doi.org/10.1038/onc.2008.394.

[101] S. Gangadhara, C. Smith, P. Barrett-Lee, S. Hiscox, 3D culture of Her2+ breast cancer cells promotes AKT to MAPK switching and a loss of therapeutic response, BMC Cancer 16 (2016), https://doi.org/10.1186/s12885-016-2377-z.

[102] B. Weigelt, A.T. Lo, C.C. Park, J.W. Gray, M.J. Bissell, HER2 signaling pathway activation and response of breast cancer cells to HER2-targeting agents is dependent strongly on the 3D microenvironment, Breast Cancer Res. Treat. 122 (2010) 35–43, https://doi.org/10.1007/s10549-009-0502-2.

[103] P. Van Der Geer, T. Hunter, R.A. Lindberg, Receptor protein-tyrosine kinases and their signal transduction pathways, Annu. Rev. Cell Biol. 10 (1994) 251–337, https://doi.org/10.1146/annurev.cb.10.110194.001343.

[104] A.C. Porter, R.R. Vaillancourt, Tyrosine kinase receptor-activated signal transduction pathways which lead to oncogenesis, Oncogene 17 (1998) 1343–1352, https://doi.org/10.1038/sj.onc.1202171.

[105] N. Prenzel, O.M. Fischer, S. Streit, S. Hart, A. Ullrich, The epidermal growth factor receptor family as a central element for cellular signal transduction and diversification, Endocr. Relat. Cancer 8 (2001) 11–31, https://doi.org/10.1677/erc.0.0080011. Endocr Relat Cancer.

[106] Y. Yarden, G. Pines, The ERBB network: at last, cancer therapy meets systems biology, Nat. Rev. Cancer 12 (2012) 553–563, https://doi.org/10.1038/nrc3309.

[107] N. Duru, M. Fan, D. Candas, C. Menaa, H.C. Liu, D. Nantajit, et al., HER2-associated radioresistance of breast cancer stem cells isolated from HER2-negative breast cancer cells, Clin. Cancer Res. 18 (2012) 6634–6647, https://doi.org/10.1158/1078-0432.CCR-12-1436.

[108] S.K. Muthuswamy, D. Li, S. Lelievre, M.J. Bissell, J.S. Brugge, ErbB2, but not ErbB1, reinitiates proliferation and induces luminal repopulation in epithelial acini, Nat. Cell Biol. 3 (2001) 785–792, https://doi.org/10.1038/ncb0901-785.

[109] M. Majumder, X. Xin, L. Liu, E. Tutunea-Fatan, M. Rodriguez-Torres, K. Vincent, et al., COX-2 induces breast cancer stem cells via EP4/PI3K/AKT/NOTCH/WNT Axis, Stem Cell. 34 (2016) 2290–2305, https://doi.org/10.1002/stem.2426.

[110] R. Roskoski, The ErbB/HER family of protein-tyrosine kinases and cancer, Pharmacol. Res. 79 (2014) 34–74, https://doi.org/10.1016/j.phrs.2013.11.002.

[111] P.J. Brennan, T. Kumogai, A. Berezov, R. Murali, M.I. Greene, HER2/neu: mechanisms of dimerization/oligomerization, Oncogene 19 (2000) 6093–6101, https://doi.org/10.1038/sj.onc.1203967.

[112] T. Holbro, G. Civenni, N.E. Hynes, The ErbB receptors and their role in cancer progression, Exp. Cell Res. 284 (2003) 99–110, https://doi.org/10.1016/S0014-4827(02)00099-X.

[113] J.A. Menendez, R. Lupu, Fatty acid synthase and the lipogenic phenotype in cancer pathogenesis, Nat. Rev. Cancer 7 (2007) 763–777, https://doi.org/10.1038/nrc2222.

[114] P.R. Pandey, H. Okuda, M. Watabe, S.K. Pai, W. Liu, A. Kobayashi, et al., Resveratrol suppresses growth of cancer stem-like cells by inhibiting fatty acid synthase, Breast Cancer Res. Treat. 130 (2011) 387–398, https://doi.org/10.1007/s10549-010-1300-6.

[115] S. Xu, T. Chen, L. Dong, T. Li, H. Xue, B. Gao, et al., Fatty acid synthase promotes breast cancer metastasis by mediating changes in fatty acid metabolism, Oncol Lett 21 (2021), https://doi.org/10.3892/ol.2020.12288.